LAPPEENRANTA UNIVERSITY OF TECHNOLOGY
LUT School of Energy Systems
Electrical Engineering

Mikko Karhunen

OVERVOLTAGE FILTERING SOLUTIONS FOR WIND TURBINE DRIVES

Examiners: Professor Juha Pyrhönen
MSc. Tuomas Stark

ABSTRACT

Lappeenranta University of Technology
LUT School of Energy systems
Degree Programme in Electrical Engineering

Mikko Karhunen

Overvoltage filtering solutions for wind turbine drives

Master's thesis

2018

80 pages, 48 figures and 10 tables

Examiners: Professor Juha Pyrhönen
M.Sc. Tuomas Stark

Keywords:

Overvoltages, differential-mode voltage, common-mode voltage, filter, d*u*/d*t*, wind power

Modern frequency converters equipped with semiconductor switches enable high switching frequencies, which along with long cables can cause harmful overvoltages to drive components. In wind turbine drives the distance between the frequency converter and the generator can be significantly over 100 meters and therefore filtering is often necessary to avoid the overvoltages.

This thesis covers the theory of the causes behind overvoltage phenomena and methods of filtering them. The objective of the thesis is to find the most effective solution for filtering both differential-mode and common-mode overvoltages. Several filtering solutions are simulated in order to compare their performance and losses. Based on the results of simulations, a diode clamped d*u*/d*t* filter is chosen to be implemented. The functionality of the filter is also proven with prototype measurements.

TIIVISTELMÄ

Lappeenrannan teknillinen yliopisto
LUT School of Energy Systems
Sähkötekniikan koulutusohjelma

Mikko Karhunen

Ylijännitteiden suodatusmenetelmät tuulivoimakäytöissä

Diplomityö

2018

80 sivua, 48 kuvaa ja 10 taulukkoa

Tarkastajat: Professori Juha Pyrhönen
DI Tuomas Stark

Hakusanat:
Ylijännitteet, eromuotoinen jännite, yhteismuotoinen jännite, suodatin, d*u*/d*t*, tuulivoima

Nykyaikaisten puolijohdekytkimillä toteutettujen taajuusmuuttajien suuret kytkentätaajuudet mahdolliset pitkät kaapelit taajuusmuuttajan ja sähkökoneen välissä voivat aiheuttaa sähkökäytön komponenteille haitallisia ylijännitepiikkejä. Tuulivoimaloissa generaattorin ja taajuusmuuttajan välimatka voi olla merkittävästi yli 100 metriä, jolloin jännitteen suodattaminen on monesti välttämätöntä ylijännitteiden välttämiseksi.

Diplomityössä käydään läpi ylijännittepiikkien syntymisen teoriaa sekä ratkaisuja niiden suodatukseen. Työn tarkoitus on löytää toimivin ratkaisu suodattamaan sekä ero- että yhteismuotoisia ylijänniteitä. Simulointien perusteella tehokkaimmaksi ratkaisuksi osoittautuneen diodeilla toteutettuun jänniteleikkuriin yhdistetyn d*u*/d*t*-suodattimen toimivuus todistetaan myös prototyyppimittauksilla.

ACKNOWLEDGEMENTS

This Master's thesis was carried out for ABB System Drives. I would like to thank the supervisors of my thesis: Nina Lagus for supervising in the beginning and Tuomas Stark for supervising at the end of the project. Thank you for all the guidance during this thesis. I would also like to express my gratitude to Pasi Puranen and Henri Kinnunen for the help I received, and Tommi Liukko and Kari Tammiaro for providing me the topic of the study.

I would also like to thank Professor Juha Pyrhönen for giving feedback and examining the thesis.

Helsinki 2.11.2018

Mikko Karhunen

Table of contents

SYMBOLS AND ABBREVIATIONS

C	capacitance
C_f	filter capacitance
du/dt	voltage rise rate
f	frequency
f_0	natural oscillation frequency
f_r	resonance frequency
G	conductance
K_p	proximity effect factor
$K_{skin(f0)}$	skin effect factor
L	inductance
L_f	filter inductance
l_{cr}	critical cable length
n	rotational speed
p	number of pole pairs
R	resistance
R_{ac}	AC resistance
R_f	filter resistance
R_{DC}	DC resistance
T_{cycle}	cycle time
t_p	propagation time
t_r	pulse rise time
u_0	initial amplitude of voltage
u_{An}	voltage between phase A and DC-link neutral point
u_{Bn}	voltage between phase B and DC-link neutral point
u_{cm}	common-mode voltage
u_{Cn}	voltage between phase C and DC-link neutral point
U_{DC}	DC voltage

u_{ge_g}	voltage between generator neutral and ground
u_{ge_o}	voltage between generator neutral and DC-link midpoint
u_{gr_o}	voltage between transformer neutral and DC-link midpoint
U_r	reflected voltage
u_U	U phase voltage
u_{Un}	voltage between U phase and DC-link neutral point
u_V	V phase voltage
u_{Vn}	voltage between V phase and DC-link neutral point
u_W	W phase voltage
u_{Wn}	voltage between W phase and DC-link neutral point
v	velocity
x	position
Z	impedance
Z_m	motor impedance
Z_x	cable termination circuit impedance
Z_0	characteristic impedance

μ	relative permeability
ζ	damping factor
Γ	reflection coefficient
ε	relative permittivity
ω	angular frequency

AC	alternating current
CCV	cycloconverter
CSI	current source inverter
DC	direct current
DFIG	doubly-fed induction generator
DOL	direct on-line drive

ESR	equivalent series resistance
FPC	full-power converter
IGBT	insulated gate bipolar transistor
LCI	load commutated inverter
PMSG	permanent magnet synchronous generator
RMS	root mean square
VSI	voltage source inverter
WRIG	wound rotor induction generator

1 INTRODUCTION

A wind turbine drive system converts the kinetic energy of wind into electrical energy that can be fed into grid. Modern wind turbines are mainly horizontal-axis wind turbines illustrated in Figure 1.1. A horizontal axis wind turbine consists of a tower, which carries the nacelle and the turbine rotor equipped with rotor blades and a hub. Some of the major components in a wind turbine drive train, such as mechanical transmission and electrical generator, are placed in the nacelle. Because of the speed control of the turbine, the generator produces an AC voltage with varying frequency. To decouple the differing frequencies of generator and grid, a frequency converter is used as an interface between the generator and the grid. The frequency converter can be placed either in the nacelle or at the bottom of the tower. [1]

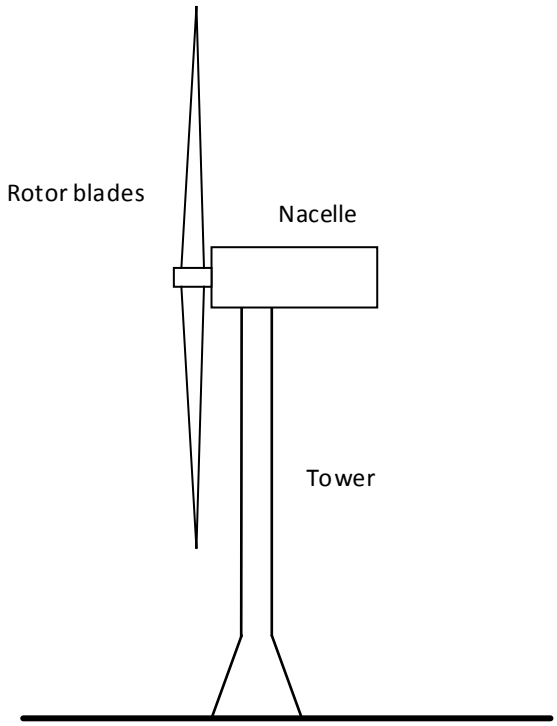

Figure 1.1 Horizontal-axis wind turbine construction. Modified from [2].

On-shore wind turbines suffer of a strong wind shear, which is caused by friction and obstacles at ground level. In high altitudes winds are stronger and wind shear caused by terrain is lower. Also, higher tower allows larger area for rotor blades, providing greater

energy yield. Therefore, a wind turbine mounted on higher tower produces more power lowering the cost of the energy produced. According to Figure 1.2 the height of wind turbine towers has been constantly increasing and the trend is predicted to still continue in the future. The height of present day wind turbine towers can be notably over 100 m. [3]

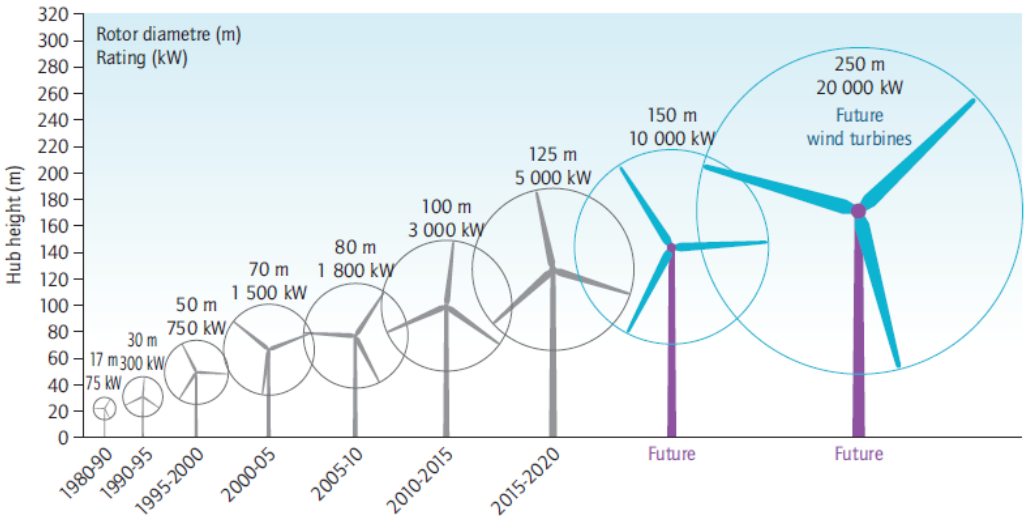

Figure 1.2 Development of wind turbine power rating, height and rotor diameter. [3]

To gain easier access to the converter for maintenance purposes etc. the converter is preferably placed on the ground level of the tower. That configuration requires a long cabling between the generator and the converter. The long cabling due to the ground level location of the converter is one factor causing overvoltage issues that form the topic of this thesis.

1.1 Wind turbine drive train

A variable speed wind turbine rotates the generator at a varying rotational speed due to fluctuating wind speed, thus producing electric power with varying voltage frequency and amplitude to the generator output. In order to provide constant output frequency and

voltage, a wind turbine drive train requires a back-to-back frequency converter system between the generator and grid. [1]

Two main concepts of variable-speed wind turbine drive trains are full power converter (FPC) and doubly fed induction generator (DFIG) that uses a partial scale power converter and a wound rotor induction generator (WRIG). In DFIG configuration, the power converter, which is placed between the rotor and the grid, is rated for approximately 30 % of the nominal power of the generator. The converter controls the rotor current, while most of the power flows between the generator stator and the grid. The low power rating of the partial scale converter results in lower losses compared to the full power converter configuration, in which all the power flowing between the generator and the grid flows through the converter. Full power converter decouples the output of the generator from the grid. Due to the decoupling of the generator stator and the grid, the FPC configuration manages more easily the grid code requirements such as grid fault ride through occasions. Furthermore, FPC enables good controllability for large range of generator rotational speed. [1]

Figure 1.3 presents the main circuit components in a wind turbine electrical drive equipped with a full power converter, which is the wind turbine drive train configuration under discussion in this thesis.

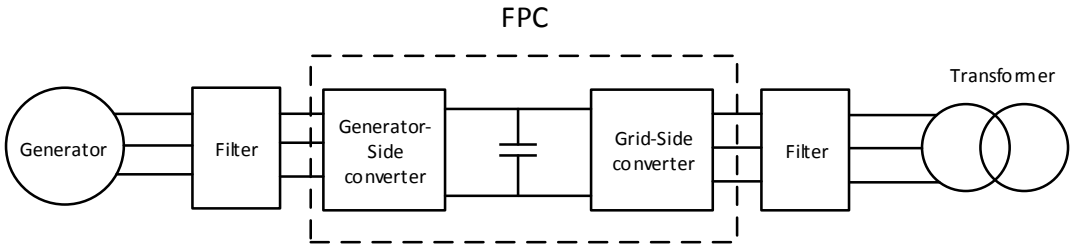

Figure 1.3 Wind turbine main circuit in drive with full power converter (FPC).

In next section, the construction and operational principle of a frequency converter will be discussed.

1.2 Frequency converter

An AC machine can be operated either as controlled or uncontrolled. If the machine does not need to be controlled, it can be operated by unregulated AC grid voltage. That is called direct-on-line (DOL) operation. The rotational speed *n* (revolutions per minute, rpm) of a synchronous machine can be calculated from equation

$$n = \frac{2f \cdot 60}{p}, \quad (1)$$

where *f* is the electrical frequency of the voltage fed to the machine and *p* is the number of pole pairs of the machine [4]. Respectively, the output frequency of a synchronous generator can be obtained by solving *f* from the equation. A variable frequency drive system enables controllability of speed and torque of the machine and has better performance and often clearly higher efficiency compared to a DOL drive. In a variable frequency drive, the frequency converter regulates the frequency and the amplitude of the voltage fed to the electrical machine.

Frequency converters can be divided to voltage source inverter (VSI), current source inverter (CSI), load commutated inverter (LCI) and cycloconverter (CCV) [5]. The most commonly used topology is VSI, which is the type of converter that will be further discussed.

A voltage-source frequency converter for motoring normally consists of three stages presented in Figure 1.4; 1) rectifier, 2) DC-link and 3) inverter [4]. The rectifier converts the AC voltage to pulsating DC voltage that is filtered in the DC-link, which also functions as an energy storage between the rectifier and the inverter. The inverter stage switches positive and negative voltages of DC-link to the motor coils in order to form the desired output voltage.

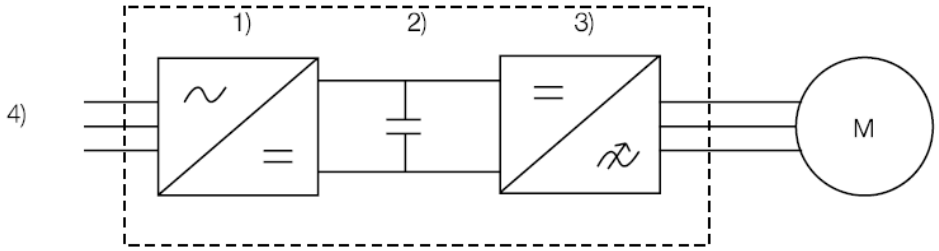

Figure 1.4 Simplified representation of frequency converter in case of a motor drive.

Voltage source inverters are typically either two-level or three-level converters. The difference between the configurations is that output of two-level inverter can be connected to positive or negative DC-link voltage, whereas three-level inverter output has an additional voltage level, 0 [5]. Out of the two configurations, two-level converter is in the scope of this thesis.

The first stage of a frequency converter is the rectifier that converts the network AC voltage into DC voltage. An inexpensive, simple and most common solution is a diode bridge rectifier, which does not require controllable components. A diode bridge rectifier arrangement is only applicable in motor drives in which bidirectional power flow is not required.

The rectified DC voltage is rippled and therefore a large capacitor is used as a filter in the DC-link of a VSI. During one half cycle of input voltage, the capacitor is charged close to peak value of the input voltage through one diode drawing high current peak and during next half cycle current through the same diode becomes zero. As a result, grid current gets highly distorted. As mentioned above, the power is only able to flow from grid to DC circuit. In wind turbine applications a power flow into grid is required and thus a solution for bidirectional power flow is used. With a rectifier bridge of controllable components such as insulated gate bipolar transistor (IGBT), bidirectional power flow and a nearly sinusoidal input current can be achieved. [6, p.79] A controlled rectifier enables the regulation of the DC-link voltage level. A controlled IGBT rectifier topology is similar as in an inverter, which is presented in Figure 1.5.

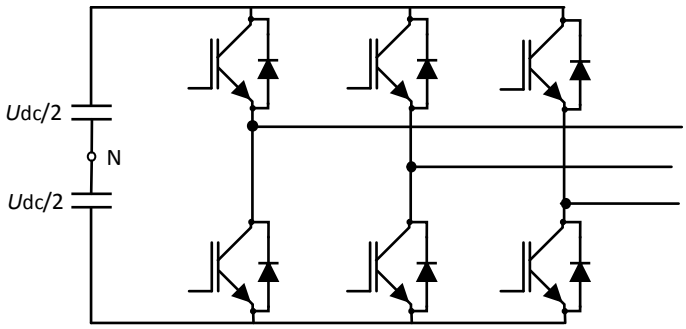

Figure 1.5 Three-phase two-level voltage source inverter.

The DC-link of a VSI can be constructed of one or more capacitors in series. The DC-link voltage U_{DC} is the voltage between the positive and the negative rail. If an even number of capacitors is used, there is a midpoint N between the capacitors as seen in Figure 1.5. The DC-link midpoint potential can be, depending on the rectifier realization, theoretically close to ground potential. However, there is practically always some ripple in the rectified DC voltage and therefore some voltage fluctuation in the midpoint potential relative to earth potential. [7]

The inverter stage of a VSI type frequency converter is supplied by the rectified voltage of the DC-link. The inverter stage consists of an IGBT bridge with six transistors, each of which with an antiparallel connected diode called freewheeling diode. The inverter topology presented in Figure 1.5 is a three-phase two-level voltage source inverter.

Inverter switches are turned on and off connecting the DC-link voltage to load generating an AC voltage waveform of the desired frequency and voltage at inverter output. The voltage pulses at the inverter output do not form a sine wave as illustrated in Figure 1.6. With inductive loads, however, the load current waveform can be close to sinusoidal. Also, an output filter can be used to achieve sinusoidal voltage.

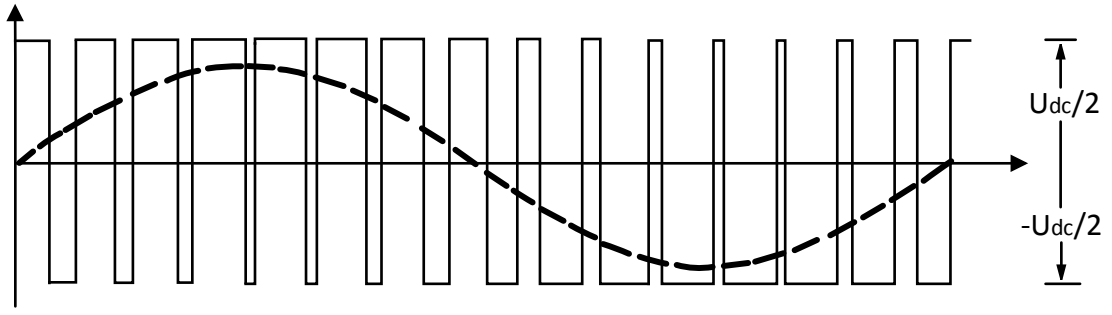

Figure 1.6 Inverter output voltage waveform. Modified from [6].

The two transistor switches of any leg of the inverter are not in the same state (on or off) simultaneously during normal operation. Thus there are eight different combinations of switch positions available. Two of the switching states produce so called zero sequence voltages, which do not generate line-to-line voltages because all phases are connected to the same potential. Table 1.1 presents the switch position combinations, resulting in output voltages of inverter phases referenced to the DC-link midpoint, voltages over motor windings and voltage at motor star point. Switch position (1,0,0) in Table 1.1 indicates that in the inverter leg of phase U the upper switch is on and the lower switch off. Respectively, in other phases upper switch is off and lower switch on. [2]

Table 1.1 Switch position combinations, resulting output voltages of inverter phases referenced to DC-link midpoint, voltages over star-connected motor windings and voltage at motor star point (n).

Switching state	Switch positions	Inverter output voltage			Motor winding voltage			U_n
		U_U	U_V	U_W	U_{Un}	U_{Vn}	U_{Wn}	
1	0,0,0	$-U_{DC}/2$	$-U_{DC}/2$	$-U_{DC}/2$	0	0	0	$-U_{DC}/2$
2	1,0,0	$U_{DC}/2$	$-U_{DC}/2$	$-U_{DC}/2$	$U_{DC}/3$	$-U_{DC}/6$	$-U_{DC}/6$	$-U_{DC}/6$
3	1,1,0	$U_{DC}/2$	$U_{DC}/2$	$-U_{DC}/2$	$U_{DC}/6$	$U_{DC}/6$	$-U_{DC}/3$	$U_{DC}/6$
4	0,1,0	$-U_{DC}/2$	$U_{DC}/2$	$-U_{DC}/2$	$-U_{DC}/6$	$U_{DC}/3$	$-U_{DC}/6$	$-U_{DC}/6$
5	0,1,1	$-U_{DC}/2$	$U_{DC}/2$	$U_{DC}/2$	$-U_{DC}/3$	$U_{DC}/6$	$U_{DC}/6$	$U_{DC}/6$
6	0,0,1	$-U_{DC}/2$	$-U_{DC}/2$	$U_{DC}/2$	$-U_{DC}/6$	$-U_{DC}/6$	$U_{DC}/3$	$-U_{DC}/6$
7	1,0,1	$U_{DC}/2$	$-U_{DC}/2$	$U_{DC}/2$	$U_{DC}/6$	$-U_{DC}/3$	$U_{DC}/6$	$U_{DC}/6$
8	1,1,1	$U_{DC}/2$	$U_{DC}/2$	$U_{DC}/2$	0	0	0	$U_{DC}/2$

As seen from the table above, the voltage U_n at the motor star point is non-zero practically at any instant of time in two-level VSI drives. The potential at the motor star point related to ground is called common-mode voltage. Common-mode voltage and its effects will be discussed later.

The operational principle of a frequency converter in a generator drive is similar to the motor drive converter explained above. In generator drive the direction of the power flow is mainly from the generator to the grid. Figure 1.7 presents the main circuit of a back-to-back frequency converter, which is a typical frequency converter topology used in wind turbine drives. Both rectifier and inverter stage of the frequency converter consist of controllable components, which are connected with a DC-link.

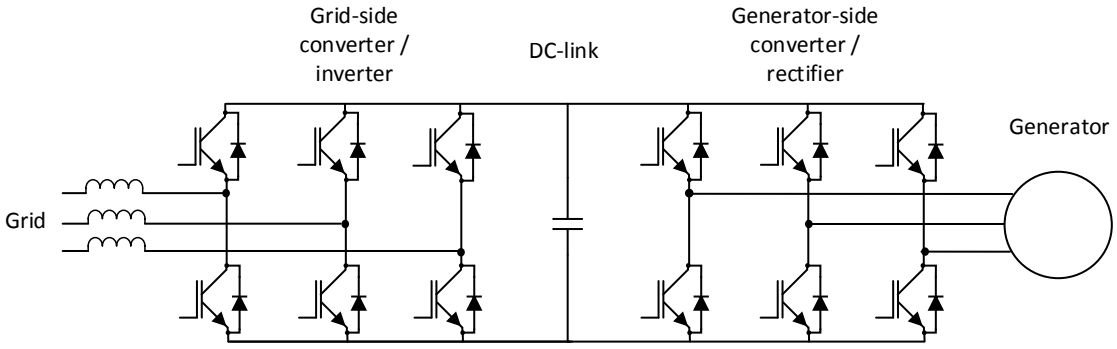

Figure 1.7 Main circuit of a back-to-back frequency converter.

In such a frequency converter, the generator-side converter is used as a controlled rectifier and the grid-side converter as an inverter converting the DC voltage into AC voltage with amplitude and frequency synchronized to the grid voltage.

1.3 The objectives and main results of the thesis

The main objective of this thesis is to develop a filtering solution for the overvoltage phenomena in wind turbine drives. The solution should be capable of filtering both differential- and common-mode overvoltages while causing as low power losses as

possible. The functionality of different filter topologies are investigated and compared by means of simulations. The filtering solution best fulfilling the requirements will be implemented as a prototype device to test it in laboratory conditions.

The filter topologies and filtering methods introduced in Chapter 3 include solutions that reduce mostly either differential-mode or common-mode overvoltages, but also solutions that aim to reduce both. In multiple studies used as references in this thesis, different d*u*/d*t* filter topologies comprising a common-mode reduction path to DC-link potential are claimed to be effective in both differential and common-mode filtering. Furthermore, combining diode clamping to d*u*/d*t* filter is claimed to improve the differential-filtering ability and to decrease the power dissipation in the filter.

Simulations verify the effectiveness of a diode clamped d*u*/d*t* filter in differential-mode overvoltage filtering. However, effective common-mode filtering would cause too high losses in filter components and therefore the objective of the prototype filter was changed to address only differential-mode voltages. According to the simulations and prototype measurements, the diode clamped d*u*/d*t* filter is effective at decreasing the differential-mode voltage peaks, while keeping the losses low compared to other solutions.

2 OVERVOLTAGE PHENOMENA IN VARIABLE FREQUENCY DRIVES

When an electrical motor is driven directly from grid, the supplied voltages can be assumed to be symmetrical, sinusoidal shaped waves without significant higher harmonic components. Unlike the voltage waveform fed to a DOL drive, inverter output voltage fed to an electrical machine is not sine wave shaped, but a continuous series of short pulses. The non-sinusoidal, high frequency pulsed nature of inverter output voltage causes several problems in the drive. Chapter 2 covers the theory of overvoltage phenomena in modern inverter drives.

Short switching times of IGBT inverters decrease the switching losses, thus reducing the cooling requirements of the inverter. Improved switching performance enables the use of high switching frequencies, which improves the waveform of inverter output voltage and current making them more sinusoidal and decreasing losses in the machine. However, high switching frequency increases losses in inverter switches. Therefore, the used switching frequency is a compromise between inverter and machine losses. [4] Switching frequencies in present-day industrial inverters are in the range of 1-6 kHz, although IGBTs could be switched with notably higher frequencies, but with derated current [6].

While the development of semiconductor switch technology has improved the efficiency of electrical machine drives, it has also brought new challenges due to high frequency pulses. Switching frequencies of several kilohertz level cause fast rise and fall times of output voltage pulses, hence high du/dt pulses of common-mode and differential-mode voltage are produced. Differential-mode noise flows from one phase to other phases with opposite directions and can be measured as a voltage between phases. Common-mode noise, instead, flows into the same direction in multiple phases and returns through common ground.

Inverter output voltage rise time is mainly determined by the characteristics of the semiconductor switches and other components of the inverter circuit. The characteristics of the cable also affect the rise time. The most usual definition for the rise time is the time in which voltage level rises from 10% to 90% of the peak value. Another important definition concerning electrical machine insulation withstand capability is du/dt, which

can be defined as the rate of voltage change during the rise time. [8] In this thesis calculation of rise time and d*u*/d*t* will be based on rise from 10% – 90% of the settled voltage value (DC-level).

As a consequence of fast rise and fall times, high peak voltages and high d*u*/d*t* values of inverter output voltage, overvoltages in cabling and machine are produced. High frequency phenomena combined with long cables may cause voltage peaks of significant magnitude. High voltage peaks can cause smalls breakdowns, partial discharges, in the air voids of insulation surrounding a conductor. Continuous exceeding of partial discharge inception voltage will slowly deteriorate the insulations and eventually cause a failure. [9]

Due to partial discharges, failures in a machine can occur from turn to turn of same coil or between coils. Because of the high d*u*/d*t* voltage is distributed unevenly over a winding of a machine. Most of the voltage drop, up to 85% of the voltage over the coil, takes place between the first and the second turn [8]. Therefore, in an inverter drive, significantly greater stress is produced on machine winding insulation compared to a DOL drive.

2.1 Voltage reflections

The output voltage of an inverter is a series of fast pulses forming an AC voltage producing about sinusoidal current in an inductive load. The magnitude of the pulses is equal to DC bus voltage at the inverter output. Modern semiconductor switching components enable, fast rise and fall times of voltage pulses as well as fast switching frequencies. Due to high d*u*/d*t* and long cabling, that is required in some installations between frequency converter and machine, the same voltage pulse that has the magnitude of the DC bus voltage at inverter output, appears higher at the machine terminals. Travelling pulses between the inverter and the machine behave like waves in a transmission line and thus the overvoltage phenomenon can be explained using transmission line theory. The peak value of the voltage at the machine terminals is defined by inverter output voltage rise time, cable characteristics, cable length and machine impedance. The reflection phenomenon happens to each pulse applied to motor. In other words, transients causing the reflections occur at every switching instant of the inverter,

and they are not dependent on the fundamental output frequency. Reflections and resulting voltage peaks at machine terminals are possible in all types of AC drives. [9]

A typical minimum pulse length for two-level low voltage IGBT converters is three microseconds. In that time, assuming that the pulse is travelling at half of the speed of light 150 m/μs, the pulse has travelled approximately 450 m by the time, when the inverter switches off the voltage pulse. 450 m is rather a long distance between an inverter and a motor, but the example points out the "slowness" of the pulse propagation in cabling compared to the rise times of IGBT inverters. These form the cause of voltage reflections in variable frequency drives. [5]

2.1.1 Motor cable transmission line model

At low frequencies, the cable between inverter and generator can be viewed as a concentrated *RL* component. The same voltage that is generated at the inverter output is usually assumed to be experienced at the machine input at the same instant. The concentrated equivalent circuit, however, does not apply to inverter drives, because of the high frequency components of the output voltage. In case of high frequency pulses, capacitive coupling between the phases, and from phases to ground occurs and thus the cable must be considered as a transmission line with distributed parameters along the cable. Transmission line model of a cable is presented in Figure 2.1. [5]

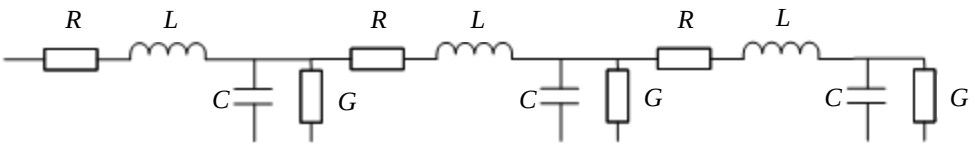

Figure 2.1 Transmission line model of a cable

Characteristic impedance Z_0 of a cable is determined by inductance, resistance, capacitance and conductance per unit length. The cable characteristic impedance is

$$Z_0 = \sqrt{\frac{R+j\omega L}{G+j\omega C}}, \quad (2)$$

where R is the distributed value of resistance of the cable (Ω/m), G conductance (S/m), L inductance (H/m), C capacitance (Fππ/m) and ω is the angular frequency of the observed signal. If the cable is assumed to be lossless, the equation can be approximated to form

$$Z_0 \approx \sqrt{\frac{L}{C}}. \tag{3}$$

Now the cable equivalent circuit may be simplified as shown in Figure 2.2

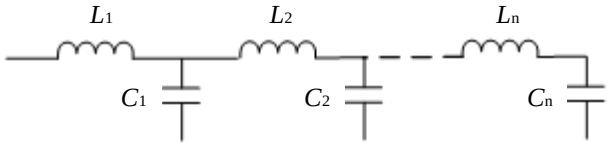

Figure 2.2 Lossless distributed parameter model of a cable.

Considering the cable as a distributed parameter model, the voltage pulse moves as a wave from the inverter to the motor end of the cable charging the capacitances. The current flowing through the last cable inductance L_n charges the capacitor C_n first to voltage U, which is the nominal output voltage of inverter. Since the impedance of the electrical machine is significantly larger than the impedance of the cable, current flowing from L_n continues charging C_n up to a higher value than U, at maximum up to $2U$ depending on the relation between cable and machine surge impedances. The impact of impedance mismatch to overvoltages will be covered in the following paragraph. The resulting overvoltage finally makes the current flow into reverse direction, from the machine to the inverter and overcharging the distributed capacitances on the way to inverter. [11]

2.1.2 Voltage reflection phenomenon

When a voltage pulse arrives at an impedance mismatch point, a reflection occurs. The relation between the incoming pulse and the reflected pulse is determined by reflection coefficient Γ. Reflection coefficient is presented as

$$\Gamma = \frac{Z_1 - Z_0}{Z_1 + Z_0}, \tag{4}$$

where Z_0 is the characteristic impedance of the cable from which the pulse is arriving to impedance Z_1. The reflected voltage U_r is a product of incoming voltage U and reflection coefficient.

$$U_r = \Gamma U \tag{5}$$

The reflection coefficient value varies between $-1 \leq \Gamma \leq 1$. Whether the reflected pulse is positive or negative with respect to the incoming pulse is determined by the sign of the coefficient. Reflection coefficient $\Gamma = 1$ is comparable to an open cable terminus from which a wave reflects with the same sign, whereas $\Gamma = -1$ compares to a shorted cable terminal producing a reflection with opposite sign. [5]

There is usually a significant difference between the impedance of machine and cable characteristic impedance. Therefore, a reflection at machine terminals is inevitable in inverter drives. At the machine-cable-junction point the reflection coefficient is usually in the range of 0.6 – 0.9. [5]

When a voltage pulse arrives from a higher to a lower impedance, the reflection coefficient is negative and therefore, the reflecting voltage continues backwards with approximately the same amplitude, but with opposite sign. A negative reflection occurs, when the incident wave from the machine arrives back to the inverter. The impedance of the DC-link capacitor at high frequencies is very low and hence the resulting reflection coefficient is approximately -1. [5]

The discontinuity point at the machine terminals is caused by the mismatch of impedances of the machine and the cable. The cable characteristic impedance varies with the cable construction and it has been experimentally determined to be in the range of 80 Ω – 180 Ω. Machine impedances have a wider scale since the rated power has a large influence on

the impedance. Based on experimental results, the characteristic impedance of an electrical machine with rated power less than 4 kW is 2000 Ω – 5000 Ω, while a 400 kW machine has a characteristic impedance of approximately 400 Ω [9].

Therefore, the reflection coefficient is highly dependent on the power rating of the machine. A machine rated for higher power has a characteristic impedance closer to that of cable. Assuming a cable characteristic impedance of 100 Ω, equation (4) gives a reflection coefficient Γ = 0.6 for a motor with 400 Ω characteristic impedance. Respectively, a low power motor with significantly higher impedance, for example 5000 Ω, gives a reflection coefficient $\Gamma \approx 0.95$ with the same cable. In that case, nearly full reflection will take place.

Although the example gave quite a low value of Γ for a 400 kW machine, it has to be considered that in high power applications, such as wind turbine drives, multiple parallel cables are often used. That reduces the apparent characteristic impedance of cabling, thus increasing the reflection coefficient. [9]

2.1.3 Machine overvoltages $\leq 2U_{DC}$

Machine terminal overvoltage caused by reflections in an uncharged cable can result in the maximum value of twice the DC bus voltage. The maximum value requires the reflection coefficient $\Gamma = 1$ between the cable and the machine. Also the cable length, pulse rise time at inverter output and pulse propagation velocity in the cable influence the magnitude of the overvoltage. Pulse propagation in a long cable can be explained as follows.

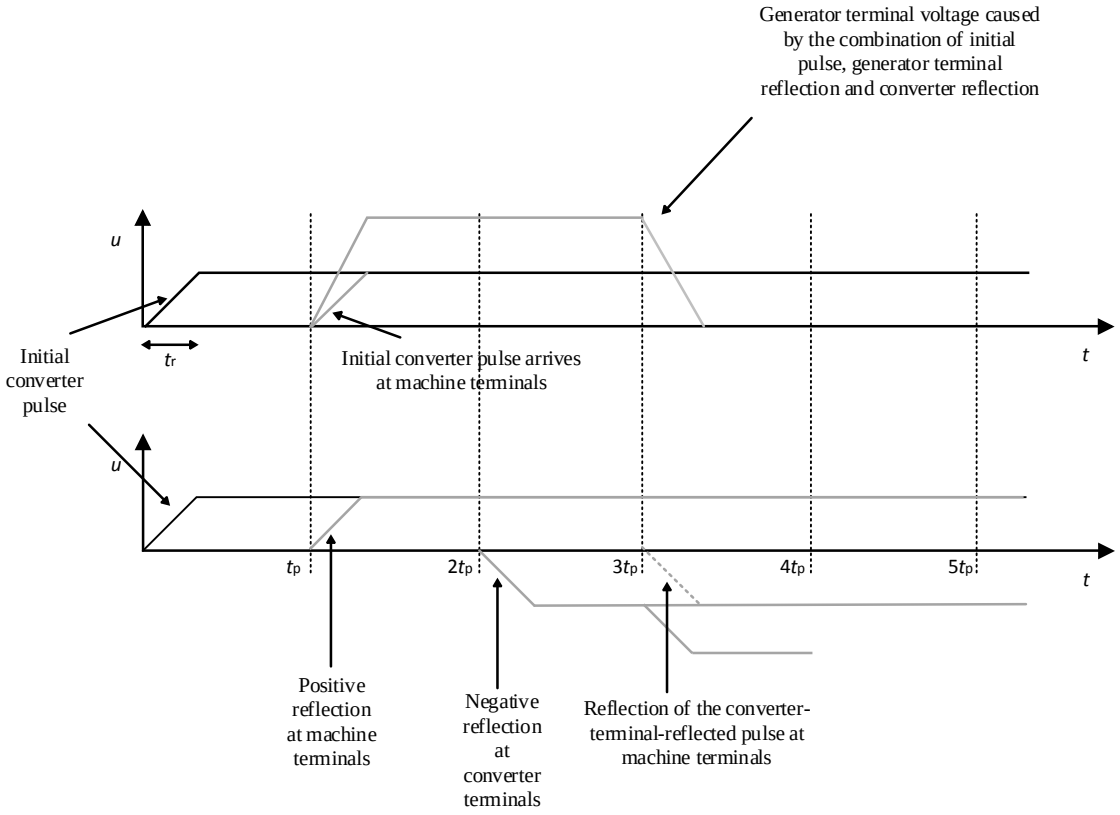

Figure 2.3 Propagation and reflections of converter pulse, and the effect to motor terminal voltage. Modified from [5].

Figure 2.3 illustrates pulses propagating between inverter and motor assuming cable-motor reflection coefficient 1 and cable-inverter coefficient −1. The amplitude of the initial converter pulse rises into the value of the DC-link voltage during rise time t_r. After propagation time t_p the initial pulse arrives at the machine terminals, where it again takes t_r for the pulse to reach the DC-link voltage. At the moment when the pulse has arrived at the machine, the reflecting pulse also begins to build up to voltage U_{DC}. As a result, the machine terminal voltage becomes $2U_{DC}$. After $2t_p$ the pulse reaches the inverter reflecting back to the motor with amplitude $-U_{DC}$, which begins to suppress the motor overvoltage at the moment of time $3t_p$. The following reflection will also affect the voltage at motor terminals generating oscillating voltage. [5]

The voltage may double at motor terminals, if the length of the cable exceeds the critical cable length. In that case the overvoltage peak will be reached before the suppressive negative voltage reflection from the inverter arrives. The critical length l_{cr} can be calculated by

$$l_{\mathrm{cr}} = \frac{t_{\mathrm{r}} v}{2}, \tag{6}$$

where t_r is pulse rise time and v is propagation velocity of the pulse. If the time in which the voltage pulse travels from motor to inverter and back is longer than the pulse rise time t_r, critical cable length is exceeded. With cable lengths shorter than l_{cr} the negative reflection from the inverter has a suppressive effect on the overvoltage at motor terminals. The more the cable length is below critical length, the more the negative pulse will suppress the peak.

The propagation speed of a wave in a cable is a result of cable's inductance and capacitance values per unit length (L_0, C_0), which are affected by the insulation material around the conductor, cable construction and conductor spacing. Widely separated conductors suspended in air have insulation relative permittivity of approximately $\varepsilon_r = 1$, which causes a propagation velocity close to the speed of light and a high natural oscillation frequency f_0. For bundled cables ε_r is higher and thus the propagation velocity and natural oscillation frequency are lower. [10]

The theoretical maximum velocity is the speed of light in case of a conductor surrounded by vacuum with μ_0 and ε_0. The following equation determines the propagation velocity v of a wave in conductor.

$$v = \frac{c}{\sqrt{\mu_{\mathrm{r}} \varepsilon_{\mathrm{r}}}} = \frac{1}{\sqrt{L_0 C_0}} \tag{7}$$

where c is the speed of light, μ_r is relative permeability and ε_r is relative permittivity. A typical value of propagation velocity in a motor cable is around 150 m/µs. [5]

The propagation time t_p, in which the pulse travels from inverter to motor in a cable of length l_c, is expressed as follows

$$t_{\mathrm{p}} = \frac{l_{\mathrm{c}}}{v}. \tag{8}$$

At the instant of time t_p, the forward travelling voltage pulse has reached the machine and will be reflected backwards with amplitude

$$\hat{u} = \frac{t_{\mathrm{p}} U_{\mathrm{DC}} \Gamma}{t_{\mathrm{r}}}, \quad \text{if } t_{\mathrm{p}} / t_{\mathrm{r}} < 1, \tag{9}$$

$$\hat{u} = U_{\mathrm{DC}} \Gamma, \quad \text{if } t_{\mathrm{p}} / t_{\mathrm{r}} \geq 1. \tag{10}$$

Therefore, if the pulse propagation time from inverter to machine is greater than the pulse rise time, the initial reflection will already have an amplitude of $U_{DC}\Gamma$. [12]

The returning negative reflection from the inverter will have a suppressing effect on the peak value of the overvoltage. The negative pulse arrives at the machine, when the initial pulse has travelled the length of the cable three times. Thus, three times the propagation time in equation (8) will be substituted to equation (9). Now the peak voltage due to the reflection can be determined by adding the incoming voltage U_{DC} to the reflected wave. [12]

$$U_{pk} = \frac{3 l_c U_{DC} \Gamma}{v t_r} + U_{DC}, \qquad \text{if } t_p < t_r/3, \tag{11}$$

$$U_{pk} = U_{DC}\Gamma + U_{DC}, \qquad \text{if } t_p \geq t_r/3. \tag{12}$$

2.1.4 Machine overvoltages > $2U_{DC}$

An overvoltage of $2U_{DC}$ occurs, when the difference between cable and machine impedance results in a reflection coefficient of approximately 1. Cable and machine impedance mismatch combined to a cable length greater than the critical length l_{cr} can cause an overvoltage up to 2 times the DC bus voltage. That applies, when an inverter pulse is applied to an uncharged cable, in other words, if the previous pulse has attenuated before the next pulse travelled to motor. However, a residual charge in a cable may lead to $3U_{DC}$ overvoltage, as the effects of the two pulses are combined. That phenomenon is called double pulsing.

The factors contributing to the amplitude of the machine overvoltage caused by double pulsing are dc-bus voltage, switching frequency, modulation technique of the inverter and natural oscillation frequency f_0 of the cable. Oscillation frequency influences the cable's damping resistance and thus the damping time of the reflected pulse. Cable's natural oscillation frequency is determined only by the characteristics of the cable and is independent of motor characteristics and pulse rise time. [10]

During one oscillation cycle T_{cycle} the wave travels four times through the cable, which means that one cycle takes four times the propagation time t_p. As shown in equation (7)

the propagation velocity v is determined by per-unit values of inductance and capacitance of the cable. The natural oscillation frequency f_0 can be expressed as follows. [10]

$$f_0 = \frac{1}{T_{\mathrm{cycle}}} = \frac{1}{4t_{\mathrm{p}}} = \frac{v}{4l_{\mathrm{c}}} = \frac{1}{4l_{\mathrm{c}}\sqrt{L_0 C_0}} \tag{13}$$

Typical value for f_0 is in the range of 50 kHz – 2 MHz [11].

The natural frequency of a cable has a significant influence on the attenuation time of a reflected wave, as it affects the AC resistance of the cable due to skin and proximity effects. Skin effect means that the inductance in a conductor is highest in the center and lowest at the surface. Therefore, high frequency current flows mostly at the surface area of a conductor having higher resistance than DC current flowing in a conductor of same width. [10]

Adjacent conductors affect each other through magnetic fields reducing the current flow area of nearby conductors. The phenomenon is called proximity effect. Due to proximity effect tightly bundled cables have greater AC resistance than separated cables. Attenuation of the pulse from initial amplitude u_0 to final value u depends on cable series AC resistance R_{ac}, characteristic impedance Z_0 and travelled distance x, as

$$\frac{u}{u_0} = e^{-(\frac{R_{\mathrm{ac}}x}{2Z_0})} = e^{-(\frac{K_{\mathrm{p}}K_{\mathrm{skin}(f_0)}R_{\mathrm{dc}}x}{2Z_0})} \tag{14}$$

where K_{p} is a factor of resistance caused by proximity effect, $K_{\mathrm{skin}(f0)}$ factor of resistance due to skin effect and R_{dc} is the DC resistance of the conductor. [10]

Due to its dependence on frequency, the AC resistance caused by the skin effect has a significant effect on the attenuation of the high frequency pulses. Equation (13) shows that the length of the cable is an affecting factor to the natural oscillation frequency f_0. The natural oscillation frequency is higher in short cables, thus resulting higher AC resistance and faster damping the shorter the cable is. [10]

Besides the damping resistance caused by the skin effect, each reflection at the machine terminals and the inverter also attenuates the transient overvoltage. As stated in paragraph 3.1.2, the reflection coefficient of low power machines is typically close to 1 and the reflection coefficient of a frequency converter approximately −1. Therefore, a standing wave is mostly damped by the cable resistance, which is relatively high because of the small diameter of the cable. However, high power drives require cabling with larger

diameter, leading to lower damping resistance. Therefore, the reduction of the voltage during each reflection multiplied by coefficient Γ becomes the dominant factor attenuating the oscillating voltage. [10]

Figure 2.4 illustrates a snapshot of the double pulsing phenomenon. Initially, the inverter and motor voltages are approximately equal. The cable is discharged and the transient is seen at the machine terminals after propagation delay of 1µs. As a result of almost full voltage reflection, the machine terminal voltage reaches nearly the negative bus voltage $-U_{dc}$. After 2 µs from arriving to the motor, the pulse has travelled from motor to inverter, reflected back with negative coefficient -1 and returned to the motor terminals. At the same moment with the negative reflection, the next control pulse has travelled the distance from inverter to motor. Coincidence of these voltages results in a peak value of almost $3U_{dc}$. Double pulsing can be avoided, if the oscillation of the previous pulse has completely attenuated before applying the next pulse.

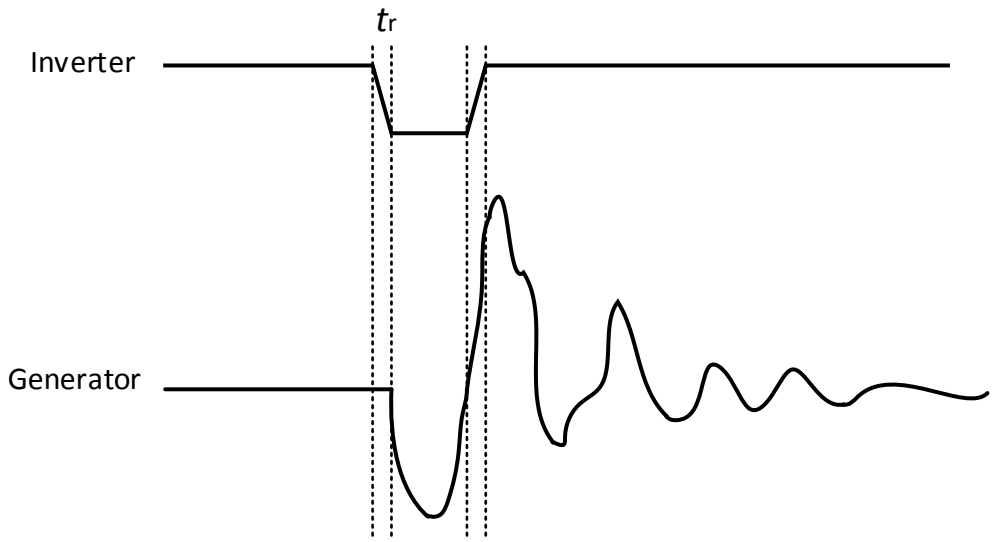

Figure 2.4 Effect of double pulsing to motor overvoltage. Modified from [5].

In addition to double pulsing, another phenomenon causing >2pu motor overvoltages, has been introduced. Polarity reversal (also referred to as double switching) may cause even higher overvoltages than double pulsing. The phenomenon causes high line-to-line voltages that occur when the modulation signals of two inverter branches are transitioned simultaneously into and out of overmodulation. That leads to polarity reversal in voltage between two phases, which can be up to $2U_{dc}$. The high voltage transient combined with

voltage reflection at motor terminals can result in overvoltages of $4U_{dc}$. Figure 2.5 illustrates double switching [5]

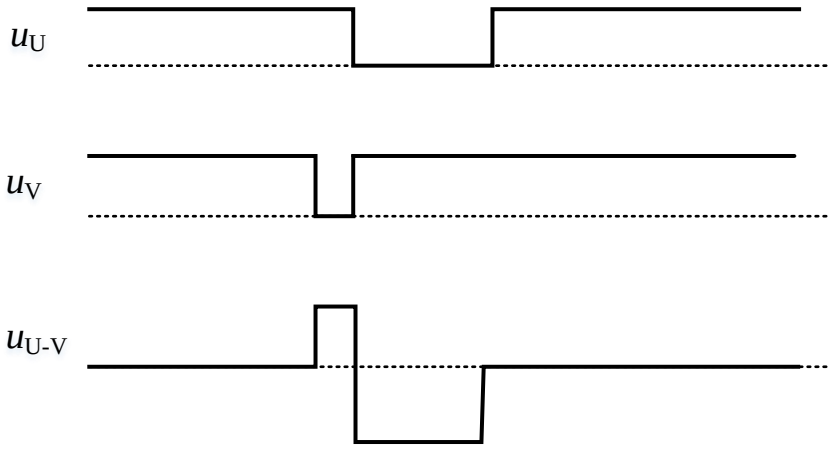

Figure 2.5 Double switching. When voltages of two phases are switched simultaneously, a high voltage spike occurs between the phases. Modified from [5].

2.2 Common mode voltages and currents

In section 2.2 the operational principle of three-phase, two-level voltage-source inverter was explained. As noted, none of the eight available switching states produce such combination of output voltages that the machine star point voltage would be zero.

During normal operation, out of six switches, three switches are on and three off. The three switches at on state can be all connected to positive or negative DC voltage, two switches to positive and one to negative DC voltage, or two switches to negative and one to positive DC voltage. When three phases of the inverter output are connected to the same potential, no differential voltage between the phases will be produced, but common mode voltage will get the maximum value.

Figure 2.6 shows an example of a pulse pattern during one fundamental frequency wave period produced by an inverter. u_U, u_V and u_W are voltages of each inverter output phase. u_{cm} is common-mode voltage, the potential at motor star point with respect to ground. It can be seen in Figure 2.6 that at some instants the potential of all three phases of the

machine is simultaneously at either positive or negative DC bus voltage. The highest peaks of common mode voltage occur, when all three conducting switches of the inverter are connected to the same potential.

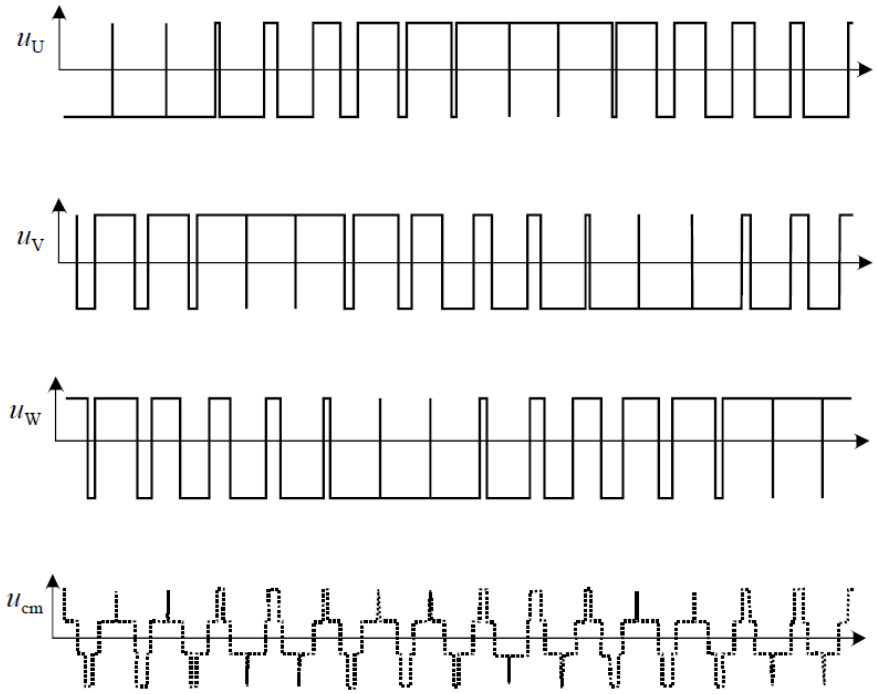

Figure 2.6 Example of inverter output pulse pattern and the resulting common-mode voltage at generator star point [4]

Common mode voltage in an inverter drive with a star connected machine can be defined as the voltage between neutral star point of the generator electrical ground. Three-phase common-mode voltage u_{cm} at the generator star point can be expressed as follows.

$$u_{cm} = \frac{u_U + u_V + u_W}{3} \tag{15}$$

In a balanced three-phase system of pure sine waves, the equation would result in common mode voltage of zero at any given instant. Any asymmetries in the voltages, however, add up to common mode voltage at the motor star point. Due to the high frequency pulsation of inverter output voltage waveform, significant common mode voltages occur in inverter fed motor drives. [6]

The common mode voltage waveform seen in Figure 2.6 can be explained with equation (15). When two phases are connected to positive DC voltage and one to negative, the resulting common-mode voltage is the sum of $(2U_{DC} - 1U_{DC}) / 3 = U_{DC}/3$. Similarly, two

phases connected to the negative rail produce common-mode voltage of $-U_{DC}/3$ However, if all phases are connected to the same potential, the equation yields either the full positive or the full negative DC voltage at motor star point.

The common-mode voltage in variable frequency drives is usually explained using a star connected machine as an example. The same principles of common-mode voltage and parasitic currents also apply to a delta connected machine, which, however, does not have a real star point at which the voltage could be measured. [5].

In section 3.1, the reflected wave phenomenon caused by long cables, short rise times and impedance mismatch between cabling and generator was discussed. When the voltage spikes occur as a result of reflections, the overvoltages can be seen in line-to-line and line-to-ground voltages. Therefore, the reflected wave phenomenon also increases the amplitudes of common-mode voltages and currents. The common-mode voltage can be approximately doubled by full voltage reflections [20].

Because of the fast rising and falling edges of the common-mode voltage, leakage current flows through stray capacitances of machine, cables, inverter and supply transformer adding up to ground path that forms the common-mode circuit. The high frequency currents flowing in the system ground can cause electrical interference in other equipment that are in connection to the same ground potential. Figure 2.7 illustrates a generator drive with stray capacitances through which the ground currents flow. [6] The LC circuit formed by the stray capacitances and the phase inductances cause high frequency oscillations in the common-mode voltage. Since the resistance in the common-mode circuit is low, the damping of the oscillations is minimal.

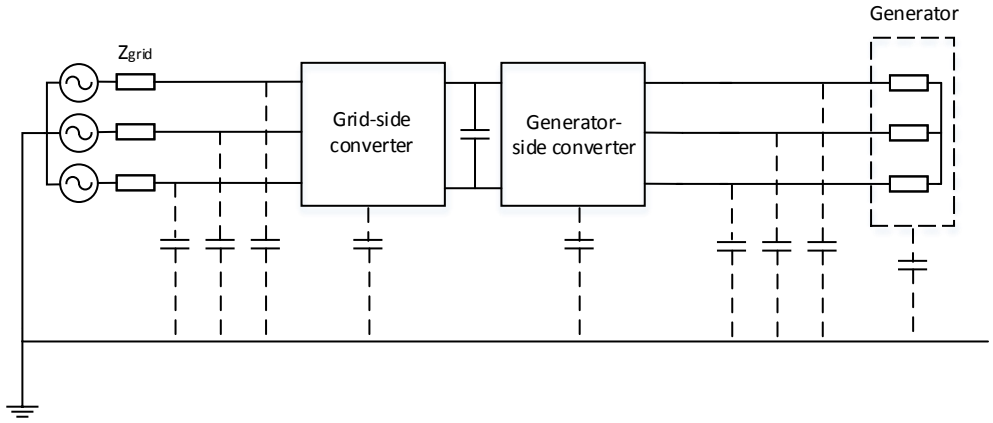

Figure 2.7 Common-mode current paths in a generator drive. Modified from [28]

Common-mode currents flowing through machine capacitances are usually paid most attention to, because of the damage they cause in the long run. There are several common-mode current branches inside the motor going through bearings. For the typical fundamental frequencies of motor phase voltage, impedance is high enough to keep the current low. High-frequency components generated, however, have significantly lower impedance path through the stray capacitances, resulting in currents that may cause failures to motor bearings. In addition to bearing currents, common-mode voltage issues can cause destructive phase-to-ground voltages at the generator side of a frequency converter, which has active converters at both grid and generator-side.

As introduced in Chapter 1, the frequency converter type covered in this thesis is full power, back-to-back wind turbine converter, which consists of two IGBT converters connected to each other via a DC-link. In such a wind turbine drive, the star point of the transformer forms a ground potential for the drive system. The common-mode noise is generated by two sources: generator-side and grid-side converter. The converters are usually operated independently and at different switching frequencies, which results in combined common-mode noise from two different sources at the generator terminals. Figure 2.8 illustrates a back-to-back converter drive common-mode circuit as one-phase representation. $u_{\mathrm{cm\_gr}}$ is the common-mode voltage generated by the grid-side converter appearing at transformer ground and $u_{\mathrm{cm\_gen}}$ is the common-mode voltage generated by generator-side converter appearing at generator star point. As the figure shows, the grid-side common-mode voltage affects the ground potential at the generator side. The filter inductance L_{f} at the generator-side converter output does not have an effect on the

common-mode noise generated by the grid-side converter. Phase-to-ground voltages may be doubled in the worst case as equation (18) points out. Therefore the common-mode voltage at generator terminals is higher in back-to-back drive compared to a configuration, where only the inverter is controllable. [14] In Figure 2.8 $e_{\text{gen\_ph}}$ is the back-electromotive force of one phase of the generator, $u_{\text{conv\_gen}}$ is the voltage of one phase of the generator-side converter and u_{phg} the voltage between generator terminal and transformer ground.

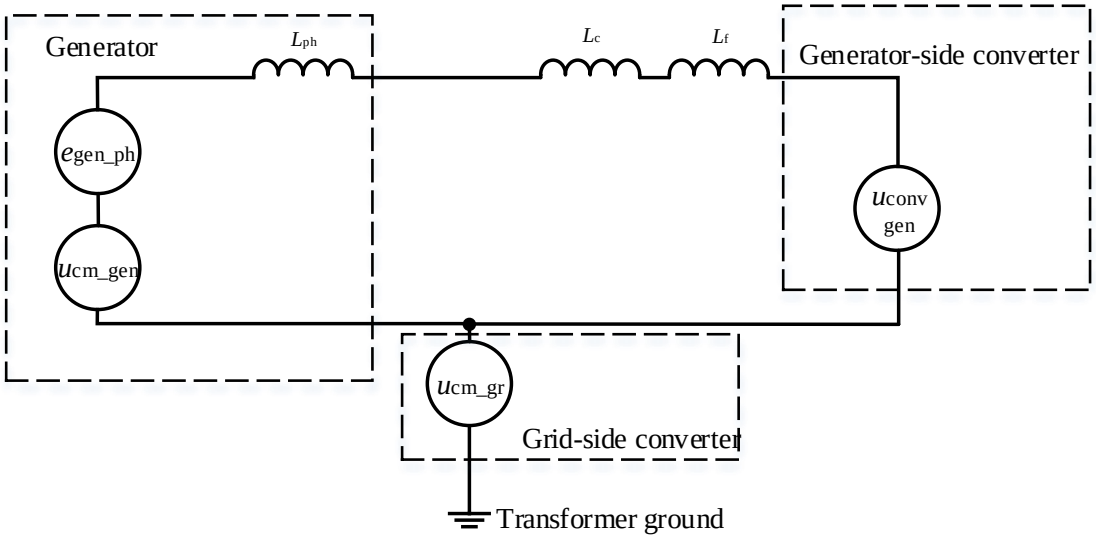

Figure 2.8 Simplified circuit describing the phase-to-ground voltages in back-to-back converter. [14]

In case of a back-to-back frequency converter, the equation of the voltage between the generator neutral and the ground potential considers the common-mode voltages produced by both converters. The following equations express the voltage $u_{\text{gen\_o}}$ between the generator neutral and the DC-link midpoint potential and the voltage $u_{\text{gr\_o}}$ between transformer neutral and the DC-link midpoint. [15]

$$u_{\text{gen\_o}} = \frac{u_{\text{Un}} + u_{\text{Vn}} + u_{\text{Wn}}}{3} \tag{16}$$

$$u_{\text{gr\_o}} = \frac{u_{\text{An}} + u_{\text{Bn}} + u_{\text{Cn}}}{3} \tag{17}$$

In (16) u_{Un}, u_{Vn}, u_{Wn} are the voltages between the generator-side phases and the DC-link midpoint and in (17) u_{An}, u_{Bn}, u_{Cn} are the voltages between the grid-side phases and the

DC-link midpoint. From equations (16) and (17) the expression of common-mode voltage $u_{\text{gen\_g}}$ between the generator neutral point and the transformer star point can be derived. [15]

$$u_{\text{gen\_g}} = u_{\text{gr\_o}} - u_{\text{gen\_o}} = \frac{(u_{\text{An}}+u_{\text{Bn}}+u_{\text{Cn}})-(u_{\text{Un}}+u_{\text{Vn}}+u_{\text{Wn}})}{3} \quad (18)$$

According to (18), the common-mode voltage may be doubled, if opposite zero-voltage vectors are applied at the grid-side and generator-side converter simultaneously. The situation can occur when the switching frequencies and the control periods of the converters are not synchronized to each other. Also a zero vector and an active vector of opposite sign at the same time cause higher phase-to-ground voltage than a single converter. By synchronizing the control of the converters, common-mode voltages can be minimized. At least zero vectors of opposite signs should be avoided. [15]

The high common-mode voltage occurring in back-to-back converter drives cannot be measured as a differential-mode voltage between phases. The most significant overvoltage spikes may appear between a phase and ground and thus the damage caused by unfiltered overvoltages are likely to occur as phase-to-ground failures.

3 FILTERING SOLUTIONS

The harmful effects of IGBT inverters have been known for a long time and several ways of mitigating the damages are developed and suggested. Usually, the degradation of insulations and bearings of a machine are the main concerns for which solutions are investigated. This study focuses on means of mitigating the adverse effects of overvoltages to insulations of generator and cabling. In some cases equipment with stronger insulations are used. To avoid the need of stronger and more expensive equipment, filtering solutions can be applied.

This chapter reviews and compares solutions introduced in literature. The aim to suppress the differential and common-mode overvoltages occurring at the generator side of a wind turbine converter with long cabling between the frequency converter and the generator. The purpose is to find a solution that is capable of providing sufficient mitigation of both differential and common-mode voltage phenomena in order to reduce phase-to-phase and phase-to-ground voltage spikes to acceptable levels in generator terminals and cabling.

3.1 Cable termination circuit at generator terminals

As discussed previously, the relation between the incoming and reflecting voltage at generator terminals is determined by the reflection coefficient Γ, which is a result of cable characteristic impedance Z_0 and the generator characteristic impedance Z_m. A cable termination network is an effective method of reducing the overvoltages caused by voltage reflections. Cable termination network is placed in parallel with the generator. The termination circuit impedance Z_x should be designed to match the characteristic impedance of the cable.

The following equation describes the reflection coefficient with a termination network.

$$\Gamma = \frac{[Z_m||Z_x]-Z_0}{[Z_m||Z_x]+Z_0} \approx \frac{Z_x-Z_0}{Z_x+Z_0} \tag{19}$$

As seen in (19) generator surge impedance does not affect the resulting reflection coefficient, when a termination network is used. In theory, a perfect impedance matching with reflection coefficient of zero would completely eliminate the reflection. [16]

Figure 3.1 shows a star connected RC circuit in parallel with a generator. Since the losses in a termination circuit implemented with only resistors would be significant, a capacitor is connected in series with each resistor. To minimize voltage overshoot, termination network should be placed close to generator terminals.

The resulting reflection coefficient is not dependent on the cable length, since the cable characteristic impedance is determined by the per-unit length values. However, filter losses increase along with the increase of inverter voltage and the length of cable. Sizing of the filter does not depend on generator characteristics or system voltage. For precise sizing of the components, the cable characteristic impedance needs to be well known. [16]

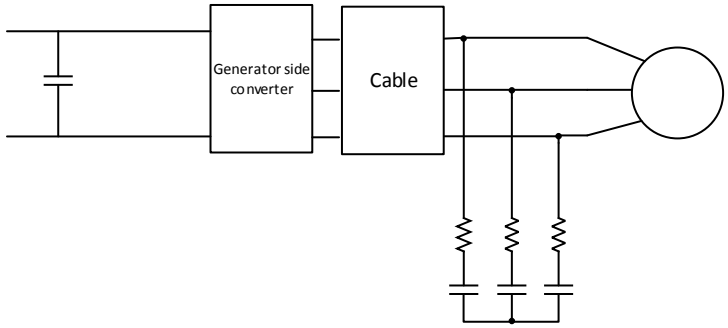

Figure 3.1 Star connected RC termination circuit

In addition to the first order RC filter, a second order LCR motor terminal filter has been introduced for example in [17]. The RC filter was demonstrated to be slightly more effective at decreasing differential-mode overvoltage peaks, whereas LCR filter causes lower losses at high switching frequencies. While a filter at machine terminals is effective at suppressing voltage reflections, it does not filter common-mode voltages or significantly limit the d*u*/d*t* value, which can also be destructive to generator. An LCR filter at converter output is claimed to better solution in terms of low losses and d*u*/d*t* limitation. [17]

3.2 d*u*/d*t* filter

A widely applied solution for filtering of both common-mode and differential-mode noise is a d*u*/d*t* filter at the inverter output. Several different topologies have been proposed in literature. A basic topology for increasing the rise time and thus reducing voltage peaks and d*u*/d*t* rate is a conventional passive LC filter that is presented in Figure 3.2. A simple LC filter consists of an inductor and a capacitor. An LC circuit causes a resonating voltage between inductance and capacitance. The resonance frequency of an LC circuit is given by

$$f_{\mathrm{r}} = \frac{1}{2\pi\sqrt{LC}}. \tag{20}$$

The resulting resonance frequency is therefore a result of inductance and capacitance values as well as the cut-off frequency, which is also affected by the resistance in the LC circuit. [7]

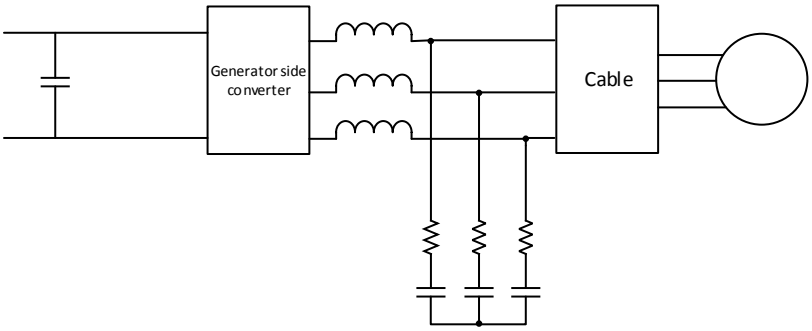

Figure 3.2 Conventional LCR filter.

The LC filter resonance may cause a large overshoot of the output voltage. The resistance of the filter elements and cabling is so low that practically the resonance must be damped by an additional resistance, which causes undesired extra losses. The capacitor series resistor's dimensioning is a compromise between the amount of losses and damping of the resonance.

An alternative, lower loss method of reducing the overshoot caused by a passive LC filter oscillation is diode clamping that will be presented later. An active LC filter can be

constructed with the same filter components as the conventional passive LC filter, but the use of damping resistors can be avoided. The avoidance of resonance overshoot is implemented by additional switching operations of existing switches in [18] or with additional switch components. The active filtering method used in [18] does not require series resistances for filter capacitors, since the overshoot and oscillation caused by fast rising and falling edges are damped by applying an additional pulse at certain moment of time before and after the actual pulse. Figure 3.3 illustrates the used pulse pattern.

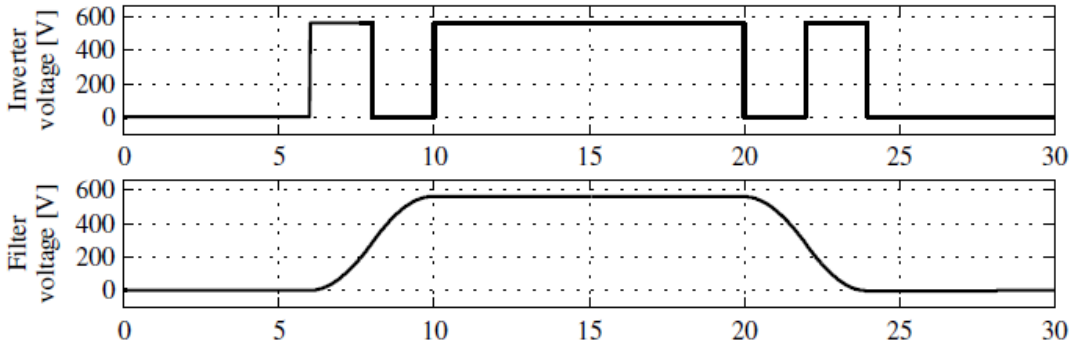

Figure 3.3 Example of inverter pulse pattern in an active LC filter. [18]

The drawback of the method is increased losses and switching frequency of converter switches as the extra switching operations are required. Also, a passive LC filter is reliable and simple to implement.

With proper dimensioning of the inductances and capacitances of an LC filter, d*u*/d*t* values rise time of the voltage pulses can be limited to a desired rate. In addition, the elimination of switching frequency harmonics can be achieved with a sinus filter, which aims to shape the inverter output voltage to a nearly sinusoidal waveform. The cut-off frequency of a sinus filter is designed to a value between fundamental frequency and converter switching frequency in order to filter out the switching harmonics. With a sinusoidal waveform the voltage reflections due to long cables could be avoided and common-mode voltage significantly reduced. [18] On the other hand, the size of a sinus filter is significantly larger than that of a d*u*/d*t* filter. In addition to large physical size and high costs the large inductance causes a significant voltage drop.

Typically, an inverter output filter has the purpose of decreasing the du/dt value of the voltage pulses in order to avoid the harmful effects to generator. For such purpose, the filter does not need to suppress the switching harmonics. Sufficient reduction of du/dt can be achieved with an LC filter with smaller values of inductance and capacitance and thus reduced physical dimensions of the components and reduced losses. An important design aspect concerning output du/dt filters is that the filter phase inductance has to be significantly lower than generator phase inductance. Otherwise the voltage drop over the filter would be excessive.

In a conventional LC filter the star point of the filter capacitors is floating and therefore the reducing effect to common-mode voltage is low. Several different topologies of LC filters for the reduction of both differential-mode and common-mode du/dt have been proposed in literature. The LC filters for DM and CM noise reduction usually use a common-mode reduction path between the star point of filter capacitors and a stable potential point in DC-link of frequency converter.

The filter in Figure 3.4 is a conventional LC filter with damping resistors and capacitor star point connected to DC-link midpoint. Common-mode voltage at generator terminals with such filter is

$$u_{\mathrm{cm}} = \frac{1}{3}\left(R_{\mathrm{f}} i_0 + \frac{1}{C_{\mathrm{f}}} \int i_0 \mathrm{d}t\right) + u_{0,\mathrm{n}} \tag{21}$$

Using very low value of filter resistances R_{f} and high value of capacitances C_{f}, the common-mode voltage could be close to $u_{0,\mathrm{n}}$, if the reflections at the generator terminals are completely eliminated. With this filter configuration, lower common-mode voltage level and smoother common-mode waveform can be achieved. Compared to the conventional LCR filter, losses are increased. [21]

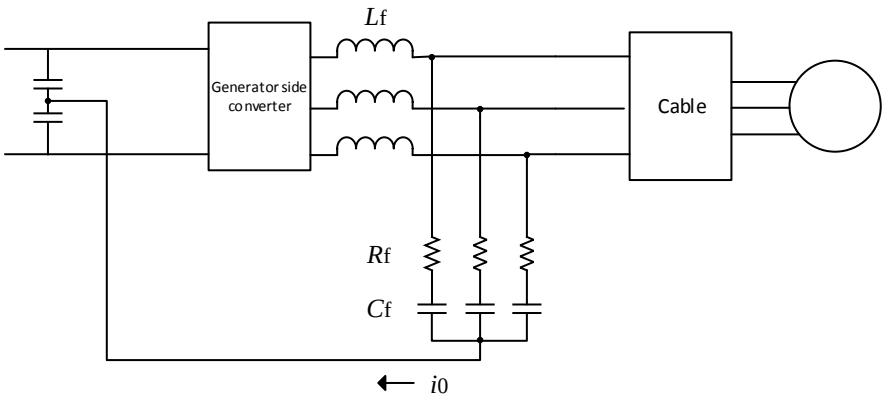

Figure 3.4 Combined differential and common-mode LCR filter.

However, the DC-link midpoint is not accessible in all frequency converters. One possible solution in such a case could be additional capacitors connecting the common-mode reduction path to the DC-link as in Figure 3.5. The potential between the two capacitors form an artificial neutral point between the positive and negative potentials of the DC-link.

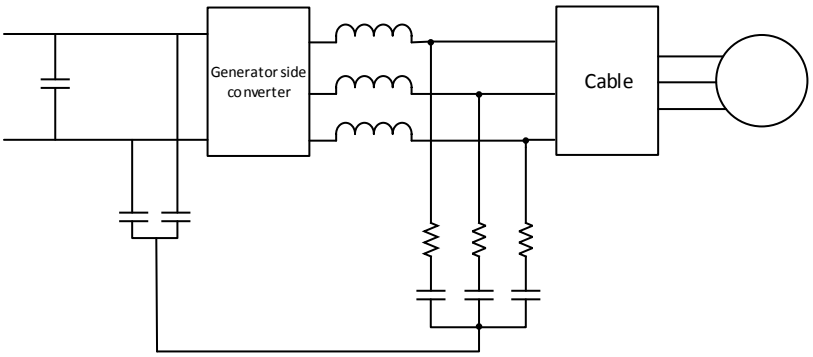

Figure 3.5 An alternative way of implementing the filter in Figure 3.4, if the positive and negative terminals of the DC-link are accessible, but DC-link midpoint is inaccessible

As discussed in section 3.2, the phase-to-ground voltages can be notably higher in case of back-to-back frequency converters. Generator-side filter cannot efficiently reduce the common-mode noise generated by grid-side converter. The filtering configuration in Figure 3.6 [21] introduces an individual LC filter for both converters. Star points of both converters have common-mode reduction path of DC-link midpoint. For issues with high

phase-to-ground voltages in a back-to-back converter that solution may be the most appropriate. Naturally, the use of two filters increases the total filtering losses.

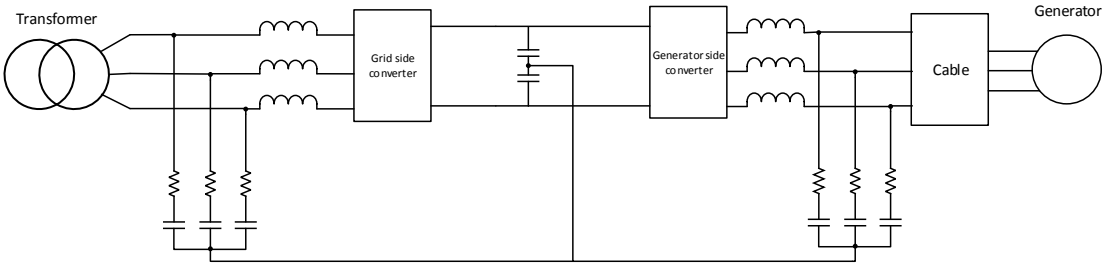

Figure 3.6 Combined differential and common-mode LCR filter at both sides of the converter.

Another LC filter solution combining common-mode and differential-mode filtering that can be implemented without DC-link midpoint connection is presented in Figure 3.7 [22]. The solution uses to RC-bridges, which are connected to the positive and negative DC-link potentials. In that case common-mode voltage at generator terminals is given by

$$U_{\mathrm{cm}} = \frac{2}{3}\left(R_{\mathrm{f}} i_0 + \frac{1}{C_{\mathrm{f}}} \int i_0 \mathrm{d}t\right) + u_{0,\mathrm{n}}. \tag{22}$$

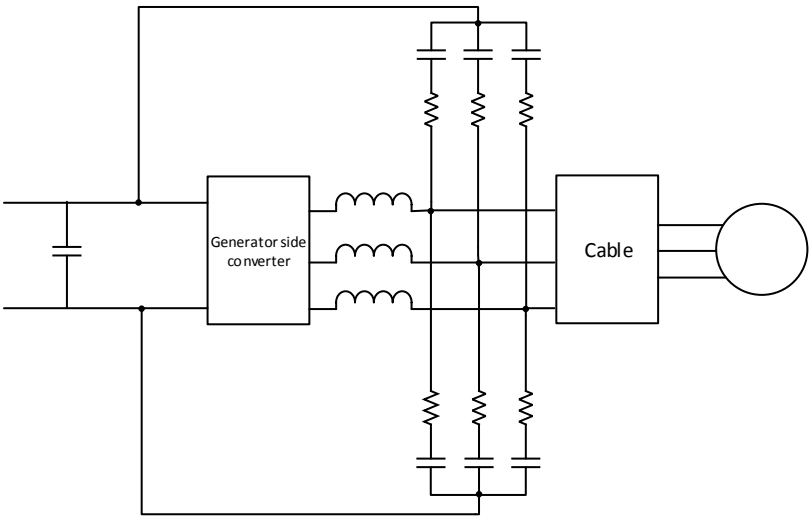

Figure 3.7 Combined differential-mode and common-mode filter with two RC-bridges.

Instead of connecting the filter star point to the DC-link midpoint or both DC-rails, also a connection to either negative or positive DC-rail is possible. In that case, neither the

access to midpoint nor two RC-bridges are required. When calculated similarly as in [20], with negative DC-link connection the common-mode voltage at generator terminals is defined as

$$u_{\mathrm{cm}} = \frac{1}{3}\left(R_{\mathrm{f}} i_0 + \frac{1}{C_{\mathrm{f}}} \int i_0 \mathrm{d}t\right) - \frac{U_{\mathrm{DC}}}{2} + u_{0,\mathrm{n}}. \tag{23}$$

Based on (23), the resulting common-mode voltage is more asymmetric (more negative compared to ground potential) than with other similar solutions that are introduced.

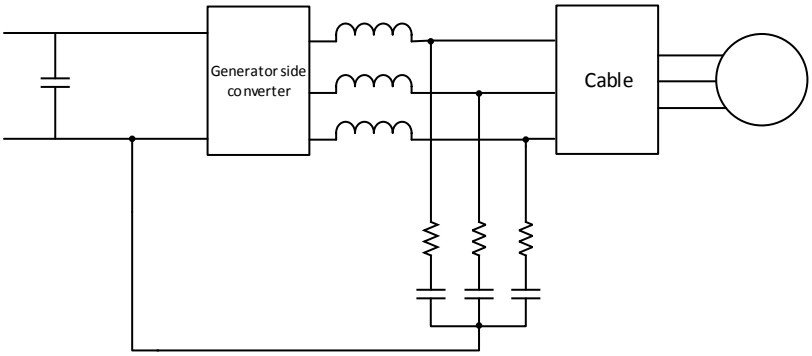

Figure 3.8 Differential- and common-mode filter in which the star point is connected to DC-link minus terminal.

Each of the configurations introduced above have essentially the same idea, a traditional LC filter with a common-mode reduction path to some DC-link potential. The stable potential connected to the star point of the capacitors reduces the d*u*/d*t* value of common-mode pulses at the generator terminals. The simplest and the most effective solution according to (21) – (23) is the one presented in Figure 3.4. The configuration, however, requires an access to the DC-link midpoint.

Also filter topologies comprising both differential and common-mode chokes have been introduced. In [23], a similar solution is proposed as in Figure 3.5, but with separate differential and common-mode inductors. A significant share of losses in LCR filters are generated in damping resistors. Several configurations using diodes to clamp the LC oscillations to the DC-link and thus preventing the use of high-loss damping resistors have been proposed.

The filter in Figure 3.9 [24] clamps the voltages higher than the positive or negative DC-link voltage at filter star point. In other words, when the voltage at the filter star point reaches either the negative or positive DC-link voltage, current starts to flow between the

filter and the DC-link. Therefore the filter losses and phase-to-phase voltage peaks may be further reduced. However, compared to the filter in Figure 3.4, common-mode filtering is not as efficient, since the common-mode reduction path is not constantly active through the diodes.

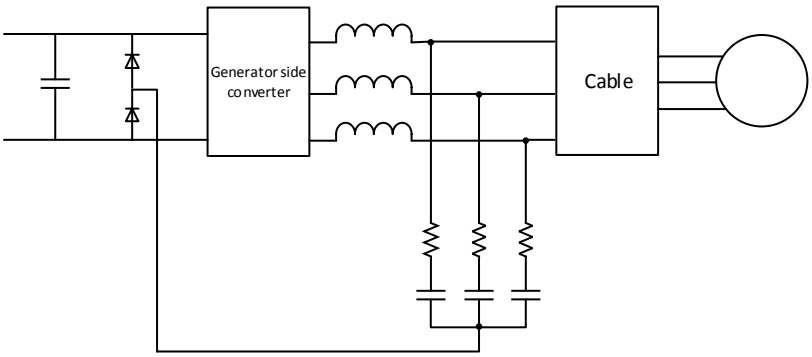

Figure 3.9 LCR filter, which connects the filter star point to DC-rails through diodes.

Filters in Figure 3.10 and Figure 3.11 use parallel diode bridge and star connected capacitors. The biggest advantage of such filters is the absence of capacitor series damping resistors and smaller size of LC components. The diode bridge efficiently cuts the oscillations of the output voltage. When the voltage at filter inductor output exceeds positive or negative DC-link voltage, a diode at the respective side starts conducting, hence cutting off the oscillating voltages and feeding the energy to the DC-link. In both LC filters with diode clamping presented below, the common mode reduction path is included. [25] The difference between the two solutions is that the filter neutral point in Figure 3.11 is connected to the DC-link midpoint instead of negative rail and without a resistor in LC circuit. In addition, that filter uses capacitors in parallel with resistors in clamp circuit in order to decrease the current stress on the clamping diodes and inverter switches.

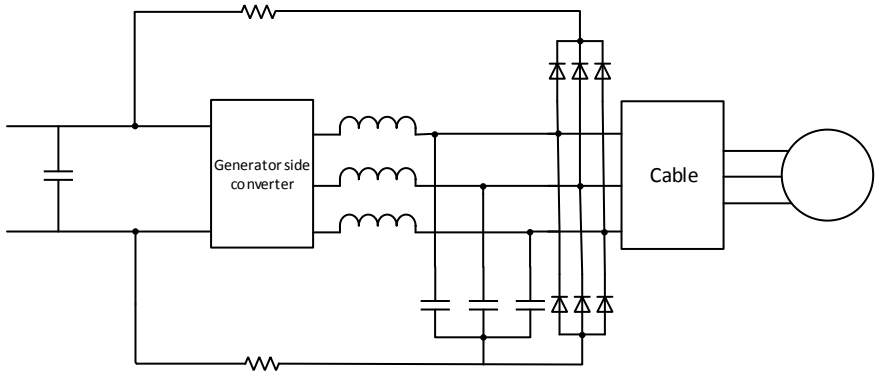

Figure 3.10 Diode clamped LC filter.

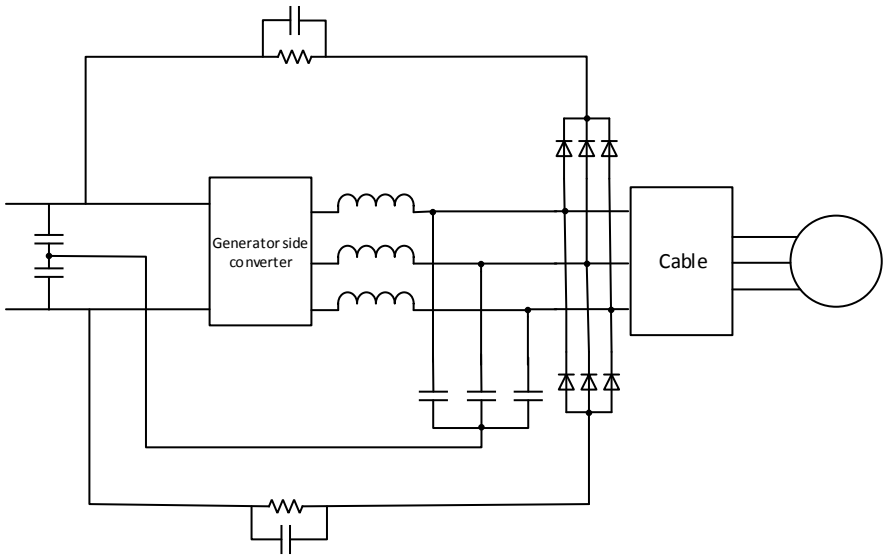

Figure 3.11 Diode clamped LC filter with DC-link midpoint connection.

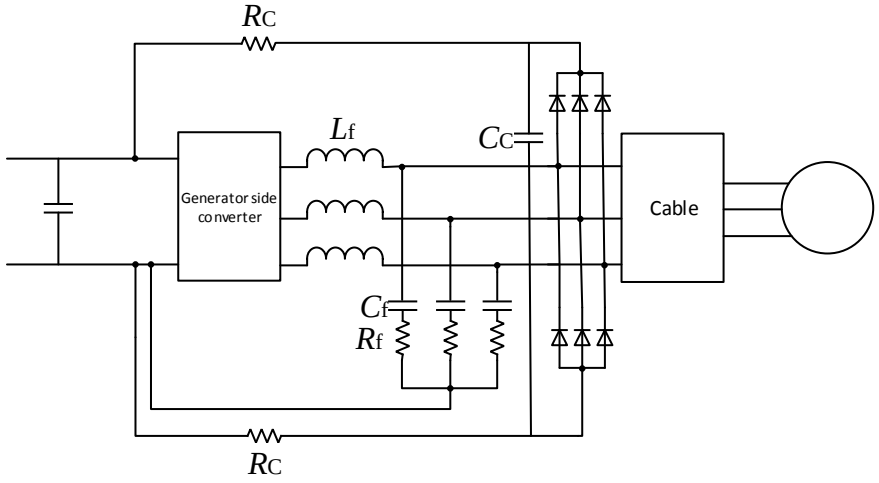

Figure 3.12 Diode clamped LCR filter, which has an additional capacitor in clamp circuit.

The filter shown in Figure 3.12 combines a conventional LCR filter and a diode clamp. The function of the capacitor C_c is to absorb the highest voltage peaks. Initially the capacitor is charged to the voltage level of the DC-link. The voltage peaks that are cut by the filter diodes increase the capacitor voltage above the DC-link voltage. The voltage between capacitor C_c and DC-link capacitor is discharged through resistor R_c.

Out of the introduced filtering solutions, passive LC filter topologies have most of the desired features: both differential and common-mode filtering, relatively low losses and simplicity. An LC filter with a connection to ground or a stable potential in frequency converter DC-link addresses both overvoltage phenomena, which makes it a widely applied solution for inverter output filtering.

The introduced passive LC filters can be divided into two groups: those where oscillations are damped with resistors (Figure 3.4-Figure 3.9) and those with diode clamping to DC-rails (Figure 3.9-Figure 3.11).

Diode clamped LC filters have the advantage of lower dissipated energy in resistors and more efficient suppression of the overshoot caused by oscillation in the LC circuit. On the other hand, as there is more energy fed back to the DC-link, problems with converter software and power rating of converter components are more likely to occur.

Active LC filters can be an effective, low-loss alternative for suppressing overvoltages. However, such a filter is much more complex to design because of the additional switching operations required. Besides, the filtering solution is intended to be an additional filter that should be relatively easy to add to an installation it is needed.

3.3 Generator common-mode voltage reduction

Another way of mitigating the common-mode voltage at generator terminals is changing the neutral point grounding of transformer. A low voltage frequency converter of a wind turbine drive is connected to medium voltage grid via a transformer. As seen from Figure 2.7 and Figure 2.8, the common-mode loop of a generator drive has a ground potential at transformer neutral point. The circuit can be reduced to form in Figure 3.13. [25]

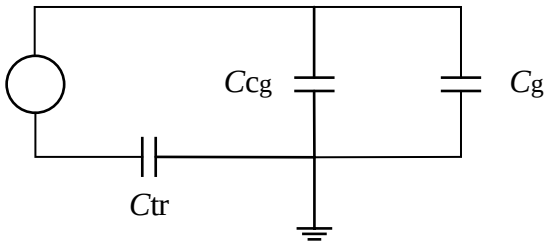

Figure 3.13 Simplified common-mode loop of a generator drive. Modified from [25]

C_g is the simplified capacitance of generator against ground, C_{cg} is the combined capacitance of cables and converter capacitance against ground and C_{tr} the ground capacitance of transformer. The high frequency common-mode voltages appearing at generator terminals can be attenuated by adding impedance to the common-mode circuit. If the transformer neutral is directly grounded, the impedance is minimal and common-mode voltage at generator is high. In case of a transformer isolated from ground, relatively small wire-to-ground capacitance C_g functions as a voltage divider, which decreases the voltage across ground capacitances at generator, cables and converter. [25]

$$u_{cm} = u_{cg}\frac{C_{tr}}{C_{tr}+C_{cg}+C_g} \tag{24}$$

An isolated transformer neutral significantly lowers the common-mode voltage at generator terminals [25]. A transformer with an isolated neutral does not have a galvanic connection to ground from the neutral point of the secondary windings. Grounding the transformer neutral point with a resistor of appropriate value would increase the impedance in the common-mode circuit, thus attenuating the common-mode voltage peaks at generator.

As equation (24) suggests, a higher value of parallel capacitances in the common-mode circuit decreases the common-mode voltage. The parallel capacitance can be increased by adding phase-to-ground capacitors to inverter output. Phase-to-ground connection provides another path for common-mode circuit, thus decreasing the common-mode stress at generator. The LCR filters introduced in the previous subsection could be also

implemented by connecting the star point to the ground potential instead of the DC-link. While the ground connection might improve the common-mode voltage mitigation, it can also have negative effects such as disturbance of ground fault monitoring due to relatively large currents fed to the ground.

4 DESIGN AND SIMULATION

The review of filtering solutions in the previous chapter concluded that the filters combining a d*u*/d*t* filter with diode clamp filters are the most effective solutions for the requirements of this work. The purpose of the simulations in this chapter is to compare different filters and their ability to mitigate differential-mode and common-mode voltage peaks.

The filters to be simulated are the alternatives presented in Figures 3.8, 3.10 and 3.12. Also a modification of Figure 3.10 without the connection from the LC filter capacitor star point to DC-minus rail will be simulated. The LCR filter without the diode clamp (Figure 3.8) is the most inefficient in terms of mitigating the overvoltages and causing low losses. However, the simplicity makes it worth of comparison to other solutions. In this chapter, the filters will be called by names pointed in Table 4.1.

Table 4.1 Filter solutions for simulations.

Filter	Figure	Explanation
Filter A	Figure 3.8	LCR filter
Filter B	Figure 3.10	LC filter + clamp
Filter C	Figure 3.10	LC filter + clamp without LC filter DC-link connection
Filter D	Figure 3.12	LCR filter + clamp

The simulations of the selected filters will be run with modelled cable length that is longer than in most wind turbines. Differential-mode voltage will be simulated with a model of 150-meter-long cables between generator and converter. Simplifying the cables into one transmission line and assuming the propagation velocity $150 \cdot 10^6$ m/s, the critical rise time of a voltage pulse is 2.1 µs given by equation (6). Hence the calculated rise time of a voltage pulse with the filter should be longer than that to avoid a full voltage reflection.

Baseline of the design procedure of an output d*u*/d*t* filter is usually the limitation of output voltage rise time or d*u*/d*t* to acceptable levels in order to reduce the reflections at the

machine terminals. Initial sizing of the filters aims to choose sufficient component values for reducing the differential-mode overvoltages. Resonance frequency of the filter should be sized to a value larger than the switching frequency. Multiple component value combinations will be simulated to find the most efficient values in terms of overvoltage reduction and power dissipation.

The transmission line between inverter and machine in the case of this thesis is constructed of cabling with low inductance and high capacitance. According to equation (3) such a transmission line has a low characteristic impedance and therefore the reflection coefficient at the machine terminals can be assumed to be high ($\Gamma \approx 1$).

The critical rise time of a voltage pulse is obtained from (6) using transmission line length of 150 m and propagation velocity of $150 \cdot 10^6$ m/s. Based on the calculated rise time, the desired resonance frequency can be approximated from [7]

$$f_\mathrm{r} \approx \frac{1}{4t_\mathrm{r}} \tag{25}$$

Appropriate inductance and capacitance values can be calculated from equation (20). Table 4.2 introduces three different inductance-capacitance combinations to avoid voltage doubling in case of a large impedance mismatch ($\Gamma \approx 1$) between the generator and the transmission line. With the proposed component values the rise time should be at the edge of critical rise time. When a conventional LCR filter is in use, the rise time should be longer for sufficient mitigation of voltage spikes. The values in Table 4.2 are intended to give approximately the size of the components for simulations.

Table 4.2 Inductance-capacitance combinations for the filter to decrease the rise time below the critical rise time, when transmission line length is 150 m.

Inductance [µH]	Capacitance [µF]
1	1.8
5	0.37
10	0.18

Large capacitance is needed for sufficient common-mode voltage reduction as shown in (21), because a larger capacitance results in lower common-mode voltage. The equation also points out that resistor value should be low to achieve low common-mode voltage.

On the other hand, with too low resistance, the oscillations of LC circuit do not get efficiently damped and therefore high peaks may occur.

Sizing of the damping resistors in an LCR filter is based on the inductance and capacitance values. The resistor should be sized so that the voltage oscillation is attenuated in as short time as possible and the overshoot is minimized. Damping factor ζ of a series RLC circuit is defined as

$$\zeta = \frac{R}{2}\sqrt{\frac{C}{L}}. \tag{26}$$

RLC circuit is underdamped, when $\zeta < 1$, critically damped, when $\zeta=1$ and overdamped, when $\zeta > 1$. The damping resistor is recommended to be sized to critical or overdamping region as equation (26) proposes.

$$R \geq \sqrt{\frac{4L}{C}} \tag{27}$$

The higher the resistance is, the lower the losses are in the filter resistors. However, excessive overdamping results in shorter pulse rise time and higher cut-off frequency, thus lowering the effectiveness of the filter. [7] Different resistor values around the critical damping resistance will be simulated to find out the best solution. It is assumed that the optimal resistance is somewhere near the critical damping value.

The main purpose of the simulations is to compare the differential-mode and common-mode filtering capability of different filtering solutions. The absolute values of the results are not expected to precisely apply in real wind turbine drives. Nevertheless, two targets for the simulations will be set: maximum voltage peak of 1.45 U_{DC} and 1.8 U_{DC}. In the simulations a large number of component combinations for each filter will be tested to find out the combinations that decrease the voltage peaks below the defined levels.

4.1 Differential-mode simulation model

The differential-mode simulation model consists of DC-link voltage, generator side converter, cables and generator. The effect of the grid-side converter to differential-mode voltages at generator is negligible and therefore the frequency converter is implemented

as a single converter model with DC-link as a simple DC voltage source with DC-plus and DC-minus levels. The converter block comprises a model of a basic two-level three-phase inverter. The pulse pattern of the frequency converter model replicates a realistic pattern of a pulse width modulated converter.

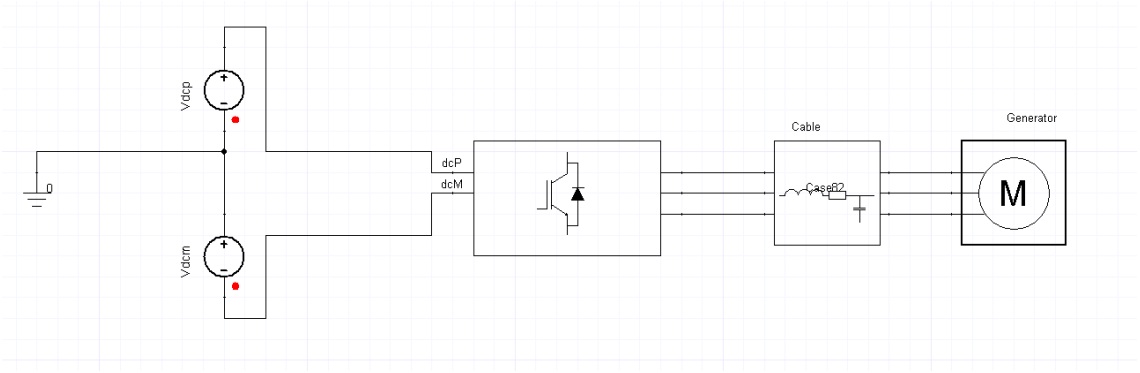

Figure 4.1 Differential-mode simulation model.

Cables are modelled as in Figure 2.2, but with resistances added in series with inductances. Therefore, the transmission line is not lossless. As in the example of Figure 2.2, the equivalent components are defined as per unit length values. The number of consecutive component blocks determine the length of cables. The generator model is a simple LR circuit with a star connected neutral point seen in Figure 4.2.

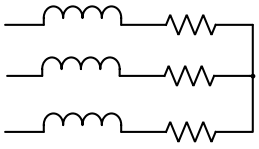

Figure 4.2 Generator model used in the differential-mode simulation model.

4.2 Common-mode simulation model

Common-mode simulation model is implemented as a one-phase model shown in Figure 4.3, which comprises the combined common-mode impedances of three phases and ground of the common-mode circuit. The voltage stimulus for the circuit is generated by four DC-voltage levels at both sides of the frequency converter. The DC-voltage sources (E1, E2, E3…) on both sides have values -1/3 U_{DC}, -1/6 U_{DC}, 1/6 U_{DC} and 1/3 U_{DC}, where

U_{DC} is the DC-voltage between the positive and the negative DC-link voltages of a frequency converter. By controlling the switches (S1, S2, S3…) and connecting a suitable combination of the DC-voltage levels to the output of the modelled common-mode circuit at certain moment of time, a waveform resembling that in Figure 2.6 is generated. The simulation model creates a setup presented in Figure 2.8, where the phase-to-ground voltage at the generator terminals is affected by common-mode voltage generated by both generator and grid-side converter. The combinations of the switch positions in the simulation model cause a pulsating voltage, which is a simulation of common-mode voltage levels without additional filtering and without the effect of long transmission line that adds to the resulting common-mode voltage.

Transformer and generator equivalent components are implemented as resistance and inductance in series. The generator star point is coupled to ground through a stray capacitance. The stray capacitances between the cables and ground and the converter and ground are also included to the model. The transformer star point is directly grounded.

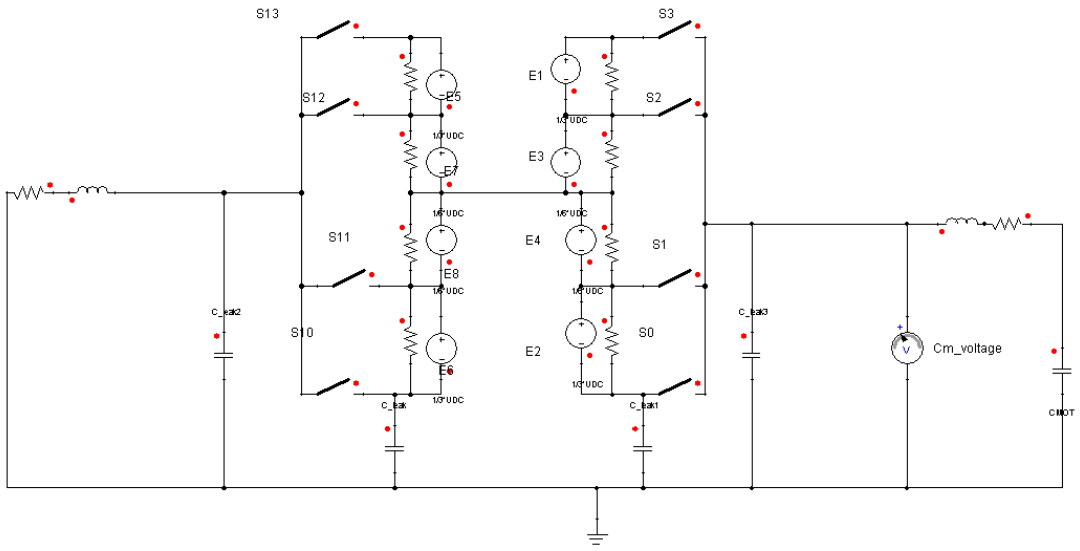

Figure 4.3 Common-mode simulation model.

The inductances and resistances of the filter in the model will be calculated as 1/3 of the value of a single component because of the three parallel phases are combined into one. Correspondingly the capacitances are multiplied by 3. The inductances and capacitances of the common-mode circuit generate oscillations to the applied voltage. The relatively

small resistance in the circuit does not have a significant damping effect on the voltage oscillations.

4.3 Simulation results

The filter solutions selected in the beginning of this chapter were applied to the introduced differential-mode and common-mode simulation models. In all the simulated filters the part which primarily addresses the common-mode voltages is the LCR filter connected to DC-link. The diode clamp primarily suppresses the differential-mode overvoltages and therefore it is not included to the common-mode simulations.

The purpose of the simulations between different solutions is to compare the resulting overvoltage amplitudes and power dissipation in filter components with different component parameters. Total loss estimation of the filter components cannot be made without knowing the resistance of the filter inductors, which generate a significant share of the losses. However, the inductors of same inductance will be used in different solutions and hence the amount of inductor losses generated by line current will not make a significant difference between the solutions under comparison. A small amount of losses is also generated in the filter capacitor equivalent series resistance (ESR), which is negligible compared to the resistance of the resistors. Loss estimation will be based on filter resistor losses.

4.3.1 Differential-mode results

To obtain comparative results of voltage peak magnitude without a filter, a short simulation was run. Figure 4.4 presents line-to-line voltage at generator terminals, when no filter is used and the length of cabling between converter and generator is 150 m. The resulting magnitude of voltage peaks is approximately 2.1 U_{DC}. The sizing of the filter that will be based on the simulation results aims to reduce the voltage peaks below the limits of 1.8 U_{DC} and 1.45 U_{DC}.

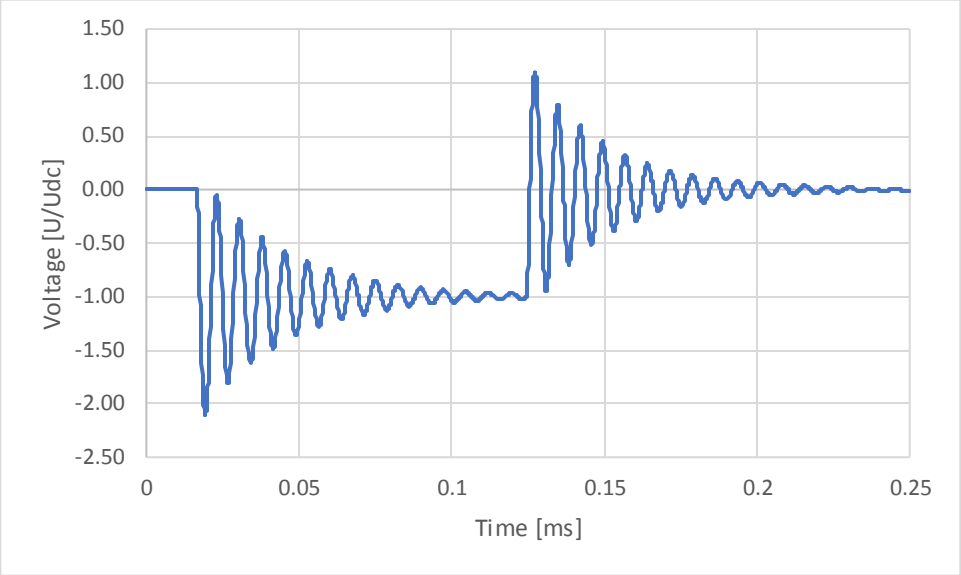

Figure 4.4 Simulated phase-to-phase voltage without additional d*u*/d*t* filtering.

The following simulation results of different filters in Figure 4.6, Figure 4.7, Figure 4.9 and Figure 4.10 present a sweep of filter parameters for the selected topologies. Phase inductances used in simulations are in the range of 2 - 16 µH and capacitances 0.1 - 2 µF. All topologies except filter A are also simulated without the RC bridge, thus forming a diode clamp filter with converter output chokes.

Damping resistors of d*u*/d*t* filters of filter A and D are sized to the critical damping value, which is calculated as in (27). Figure 4.5 shows simulations of voltage peaks as a function of LCR filter damping resistor value in case of filter A. Simulation results suggest that lowest value of voltage peak is achieved, when a resistance close to the critical value is used. Therefore, the resistance value used in the following series of simulations will be the critical damping value. Table 4.3 shows the critical damping resistor values for the component combinations used in the simulations of Figure 4.5.

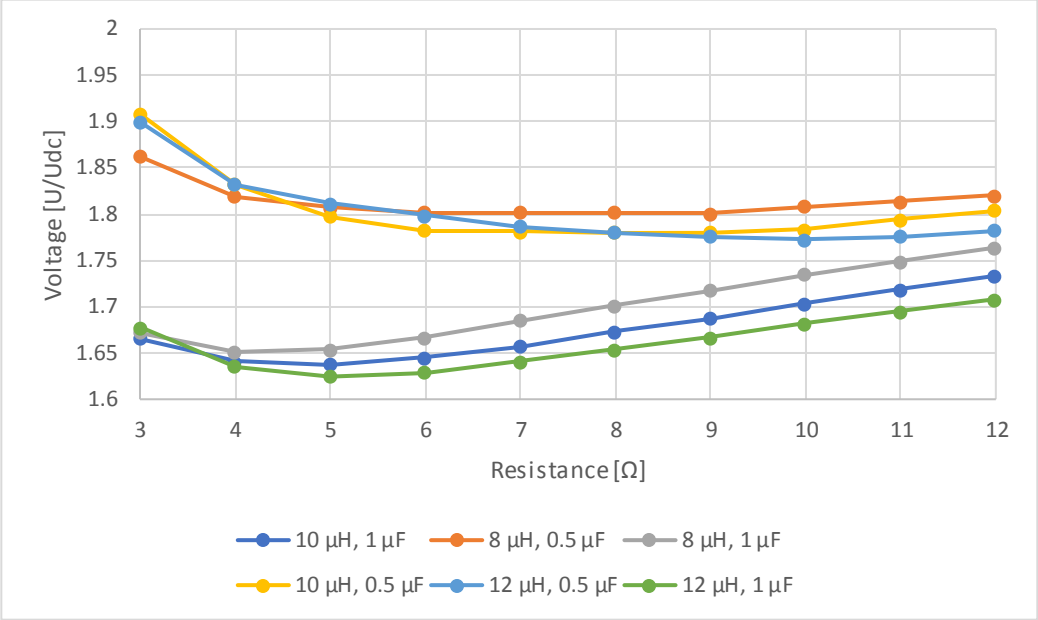

Figure 4.5 Dependency of voltage peak magnitude and LCR filter resistance with different filter inductance and capacitance values.

Table 4.3 Inductance and capacitance values used in simulations of Figure 4.5 and their corresponding resistor values for critical damping.

L, *C* values	sqrt(4*L*/*C*)
8 µH, 0.5 µF	8.0
8 µH, 1 µF	5.7
10 µH, 0.5 µF	8.9
10 µH, 1 µF	6.3
12 µH, 0.5 µF	9.8
12 µH, 1 µF	6.9

In filter D the large capacitance C_c has a significant effect on the optimal resistor value. In spite of that, the same equation is used to the resistor value calculation of filter D. If filter D turns out to be the best solution, the resistor value will be optimized.

Maximum voltage peaks and losses of filter A with a wide range of simulated component values are shown in Figure 4.6. Filter A appears to be inadequate to mitigate the magnitude of the voltage peaks below 1.45 *U*dc. The combination of 16 µH inductance and 2µF capacitance reaches almost the desired level, but resistor losses are approximately 16 kW. Also, a choke with inductance of 16 µH is quite large and heavy for drives of megawatt range.

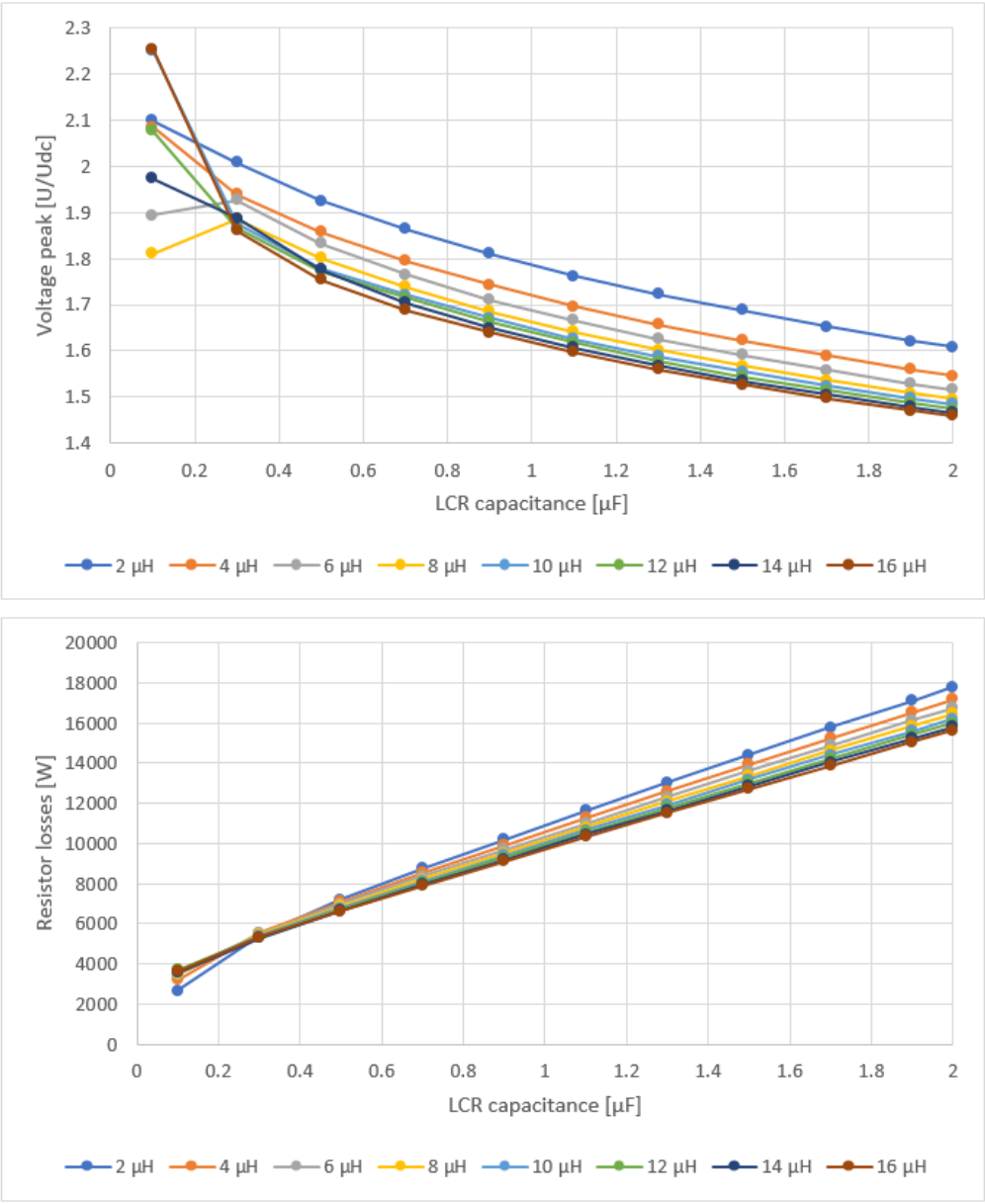

Figure 4.6 Maximum voltage peaks at generator terminals and resistor losses of Filter A with different component combinations.

Figure 4.7 introduces the simulated maximum voltage peaks and resistor losses of filter D. The losses are calculated from both the LCR and clamp filter resistors. The losses are approximately equal to those of the previous filter, but maximum voltage peaks are significantly lower.

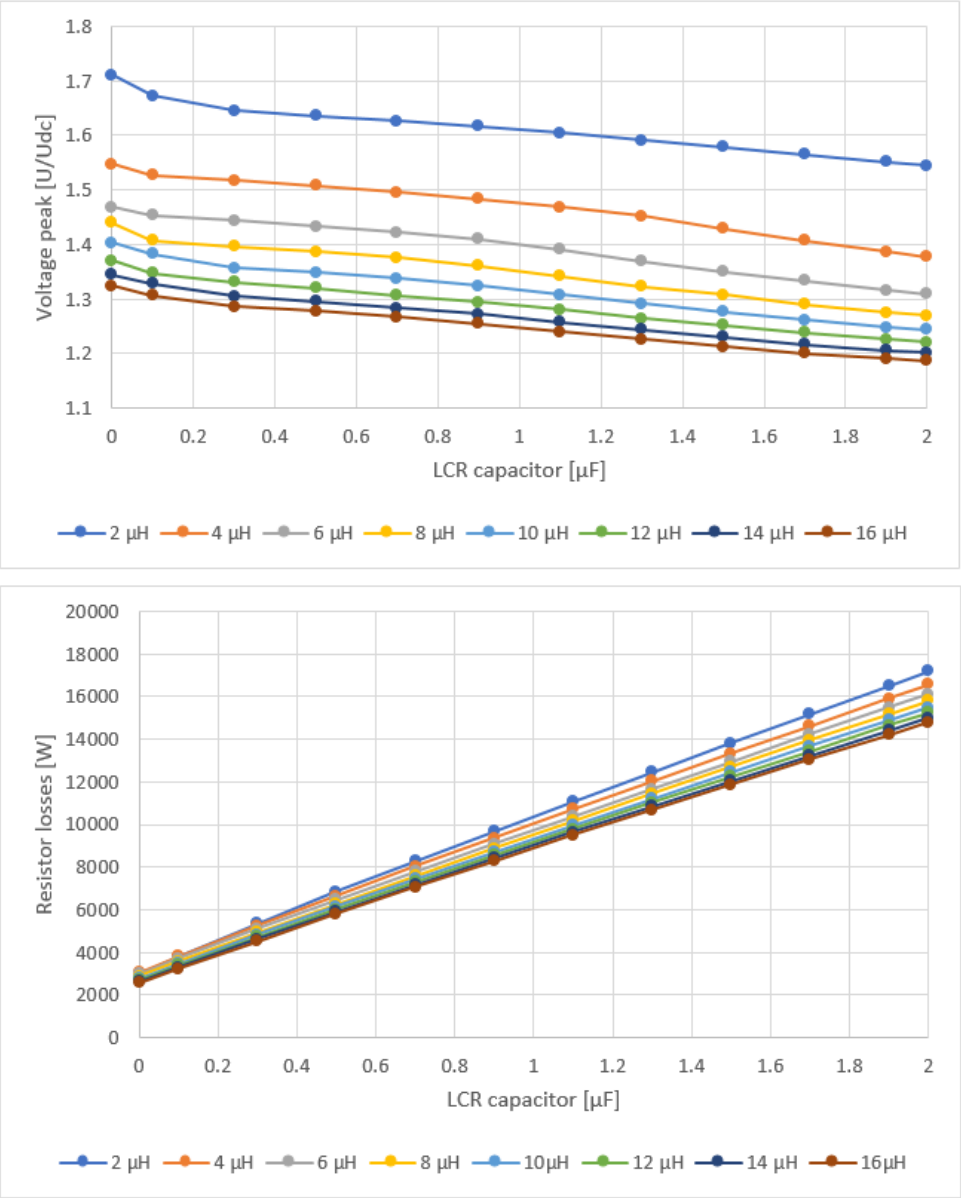

Figure 4.7 Maximum voltage peaks at generator terminals and resistor losses of Filter D with different component combinations.

Figure 4.8 compares the waveforms of filter A and filter D. LCR components in both filters are 8µH, 0.5 µF and 8 Ω. The oscillation is suppressed in a notably shorter time than in the case without filtering in Figure 4.4. The diode clamped filter has a result of lower voltage peak and more effective damping of the oscillation, which however, is more predictable in the LCR filter without the diode clamp.

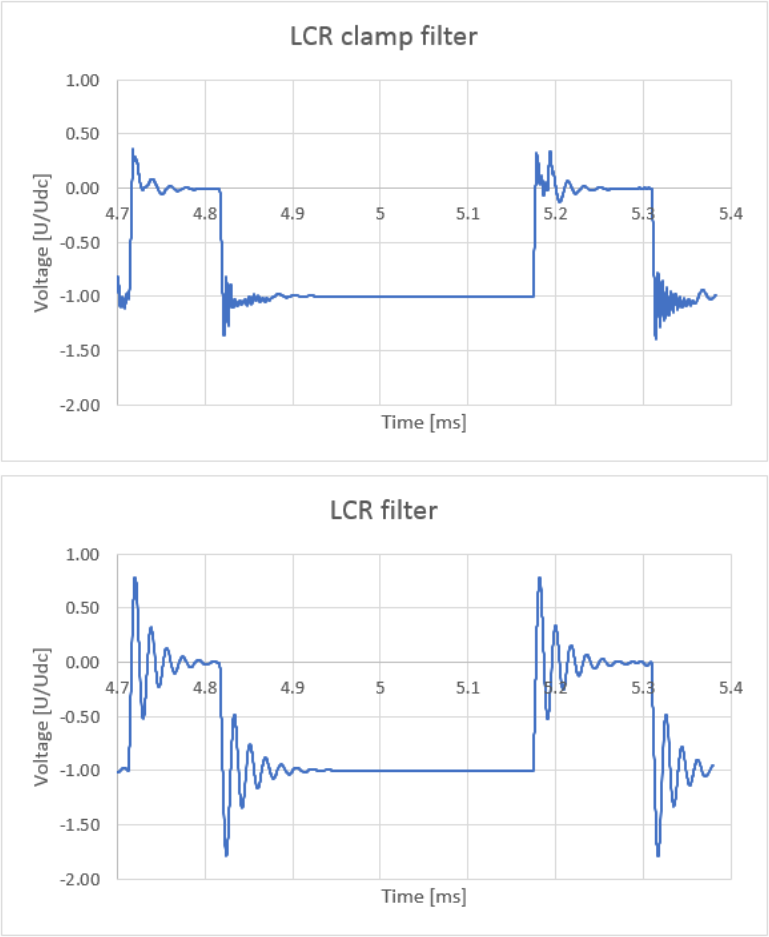

Figure 4.8 Simulated voltage pulses and the oscillation at generator terminals with filter D (LCR clamp filter) and filter A (LCR filter)

Comparison of the conventional LCR filter and the diode clamped LCR filter proved that the clamp filter is more efficient in filtering differential-mode voltage spikes. Next, the simulation results of the two remaining solutions are presented. The first diode clamped filter under inspection is the one in filter B with the DC-link connection from the LC filter star point in Figure 4.9. Figure 4.10 presents the results of simulations of the filter C. The differences in maximum voltage peaks are not significant between the two filters. Filter D results in consistent decrease of voltage, when either inductance or capacitance is increased, whereas filters B and C have much more inconsistent output. That is likely a result of the absence of damping resistors. Therefore, some inductance-capacitance combinations cause oscillations that are not effectively damped. The most notable difference between filter B and filter C is the steeper rise of losses in filter C, when capacitance is increased.

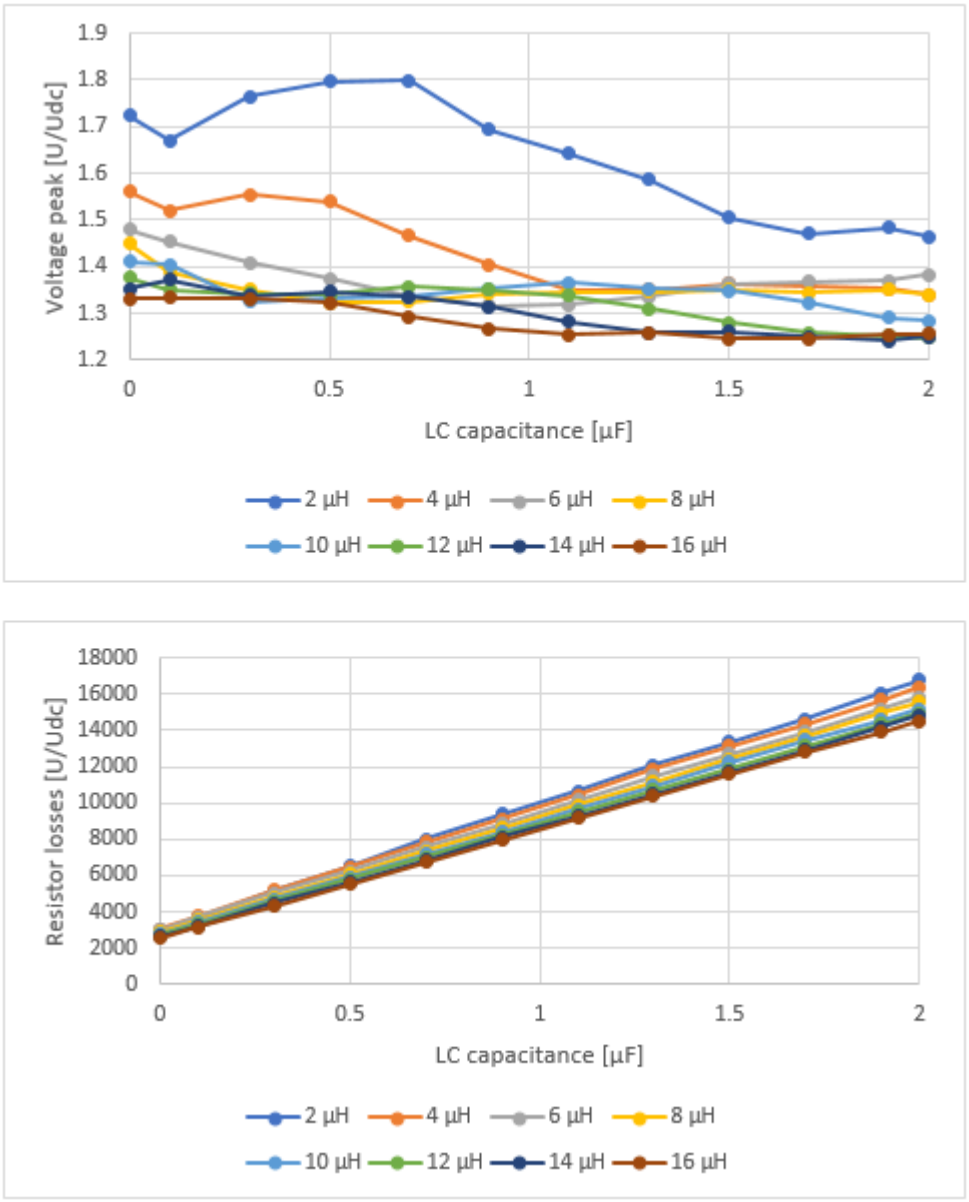

Figure 4.9 Maximum voltage peaks at generator terminals and resistor losses of Filter B with different component combinations.

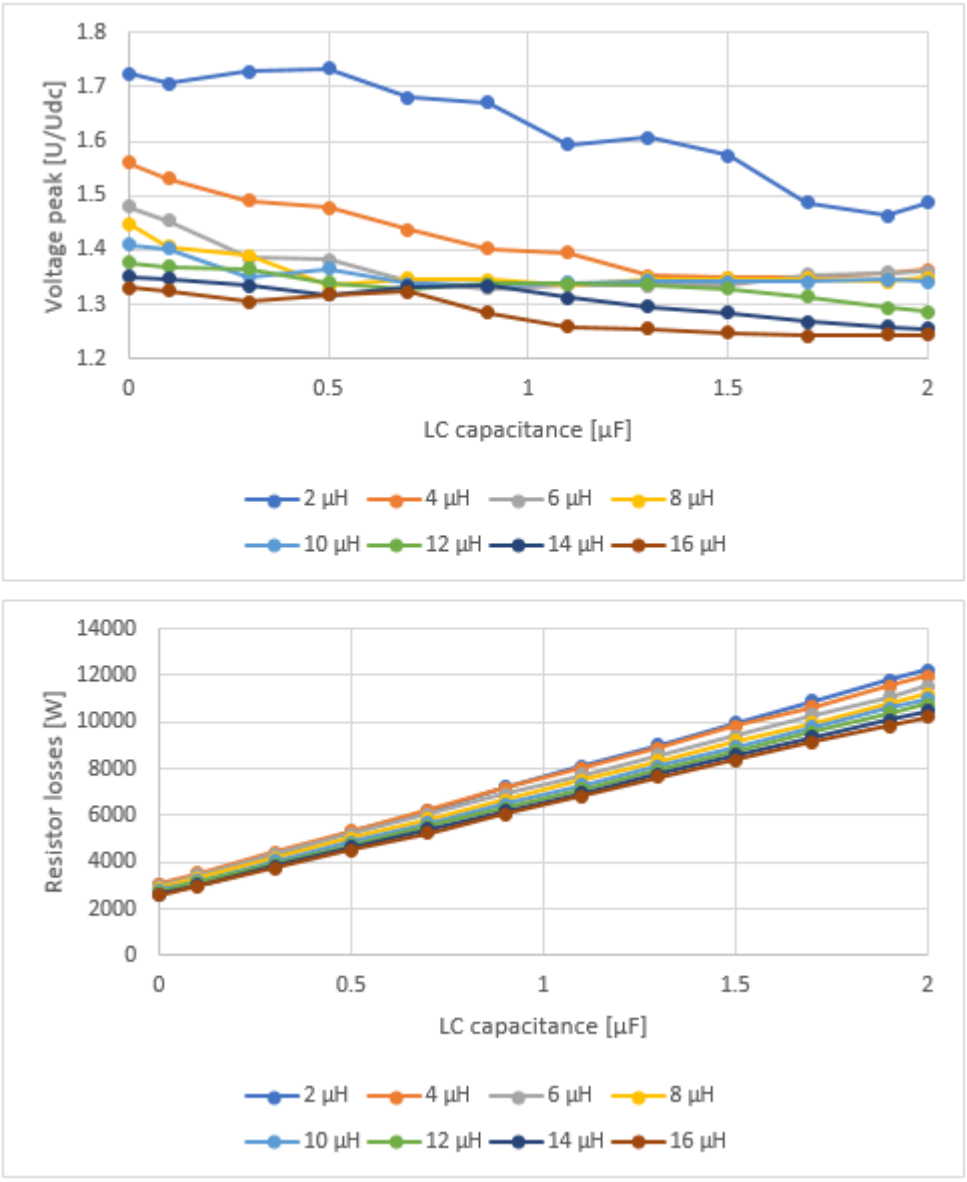

Figure 4.10 Maximum voltage peaks at generator terminals and resistor losses of Filter C with different component combinations.

Table 4.4 compares the results with different filters in cases that decreased the voltage peaks to 1.45 U_{DC} or below. In case of filter A the maximum voltage peak of less than 1.45 U_{DC} was not achieved and therefore the results closest to that are presented. The results of the three filters with diode clamp do not significantly differ from each other. In turn the efficiency of filter A is far from others. Although the diode clamped filters are quite even in the comparison of Table 4.4, the predictability of filter D makes it a better solution compared to others. Furthermore, common-mode filtering ability is assumed to

be highest in filter D, especially compared to filter C, which does not include a connection from d*u*/d*t* filter star point to DC-link.

Table 4.4 Component combinations which suppress the voltage peaks below 1.45 U_{DC} for each filter. Note that filter A did not decrease the highest voltage peaks under the limit even with the highest inductance and capacitance.

Filter	Capacitance [µF]	Inductance [µH]	Voltage peak [U/U_{DC}]	Resistor losses [W]
Filter A	2	16	1.46	15621
Filter B	0	8	1.45	2872
	0.3	6	1.41	5001
Filter C	0	8	1.45	2870
	0.3	6	1.39	4317
Filter D	0	8	1.44	2871
	0.3	6	1.44	5103

As mentioned, the used resistor values in the previous simulations for filter D were not optimally designed. The following figures show a closer investigation of the effect of d*u*/d*t* filter resistance value to voltage peaks and resistor losses.

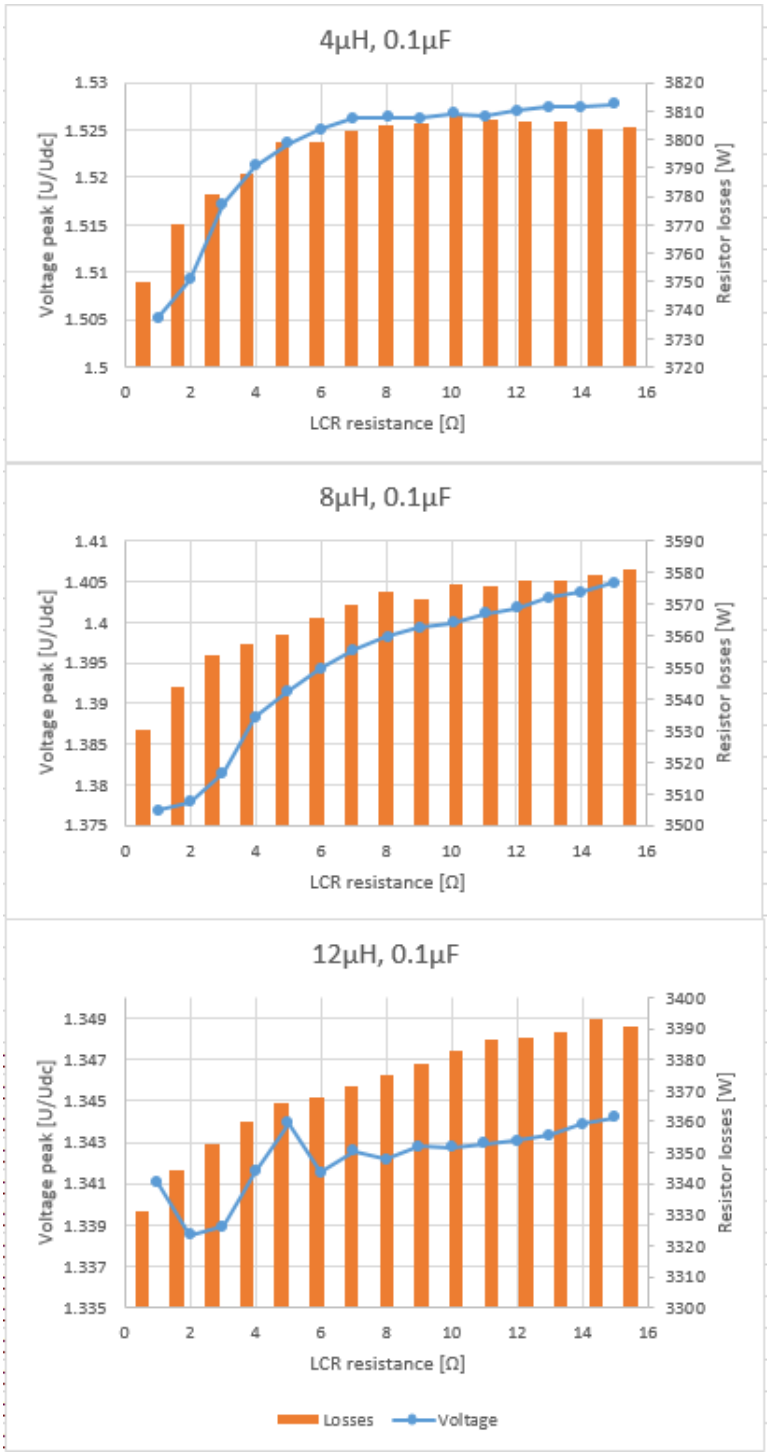

Figure 4.11 Maximum voltage peaks and resistor losses as a function of resistance with 0.1 µF capacitance and three different values of inductance. The y-axis values are scaled individually to each graph.

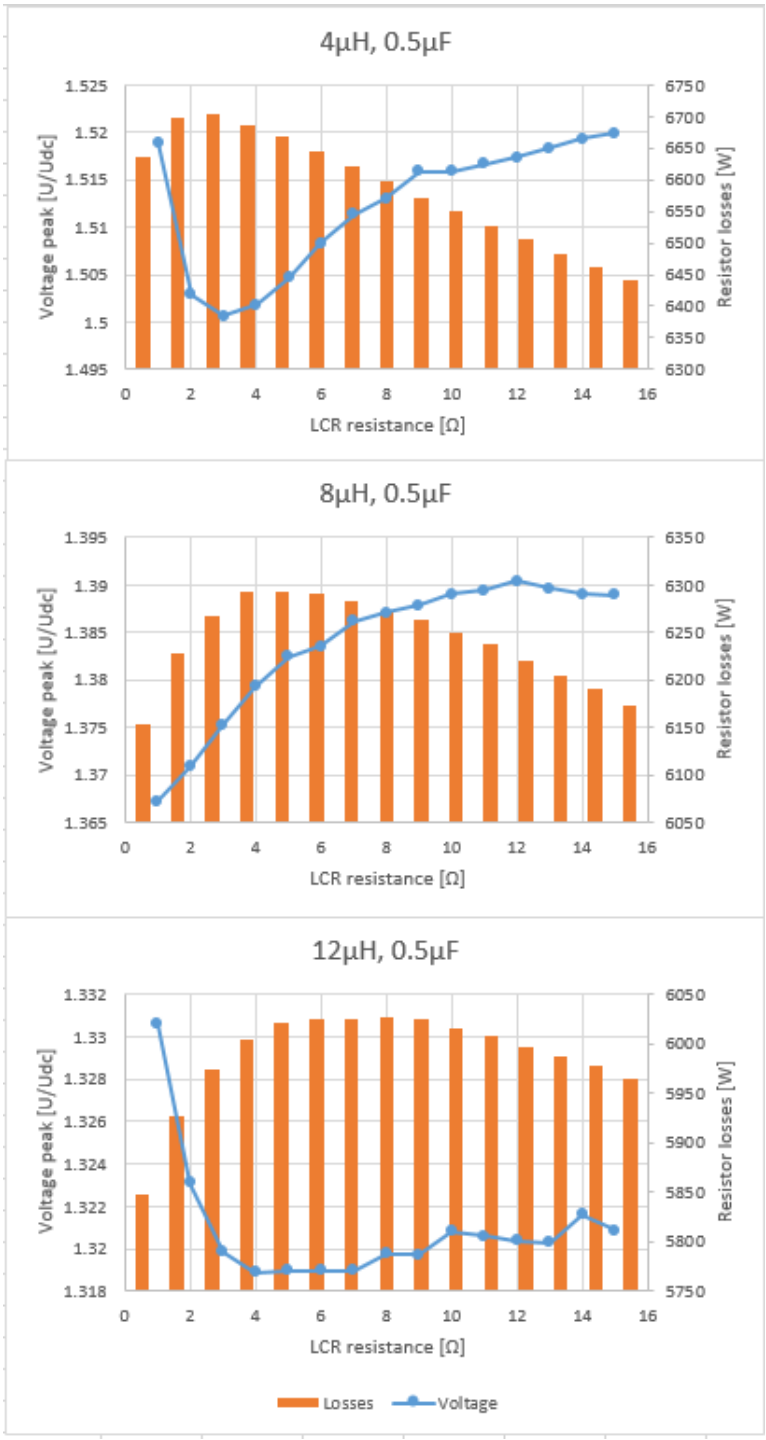

Figure 4.12 Maximum voltage peaks and resistor losses as a function of resistance with 0.5 µF capacitance and three different values of inductance. The y-axis values are scaled individually to each graph.

Examination of Figure 4.11 and Figure 4.12 shows only a slight difference between the highest voltage peaks of the same filter with 0.1 µF and 0.5 µF capacitors. Note that each of the graphs are individually scaled. Although the higher values of capacitance decreases the voltage peak slightly, the resistor losses at the same time almost double. Based on that

increasing the capacitance from 0.1 µF to 0.5 µF does not appear to have enough profit compared to the amount of losses.

Figure 4.11 and Figure 4.12 show the influence of the value of LCR filter resistors to the voltage peaks and the combined losses in all resistors in the filter circuit. Equation (27) does not apply in this case because of the large capacitance C_c in the clamp circuit. It can be seen that the total losses do not change significantly along with the variation of the LCR filter resistance. The simulation results show a rising trend of voltage spikes as the resistance increases. In terms of voltage peak magnitude, a small resistance value seems to be optimal, not zero however. Yet it should be noticed that with a small LCR filter resistance, most of the resistor losses take place in the clamp circuit resistors. Furthermore, the maximum current capacity of LCR filter capacitors must be considered, when determining the resistance value. Higher resistance leads to lower current through the RC bridge components and therefore the components could be downsized.

4.3.2 Common-mode results

Figure 4.13 shows the common-mode voltage waveform at the generator terminals given by the simulation model, when filtering is not applied. The oscillation of the voltage causes occasional high peaks of which maximum and minimum values are 1.44 U_{DC} and -1.46 U_{DC}.

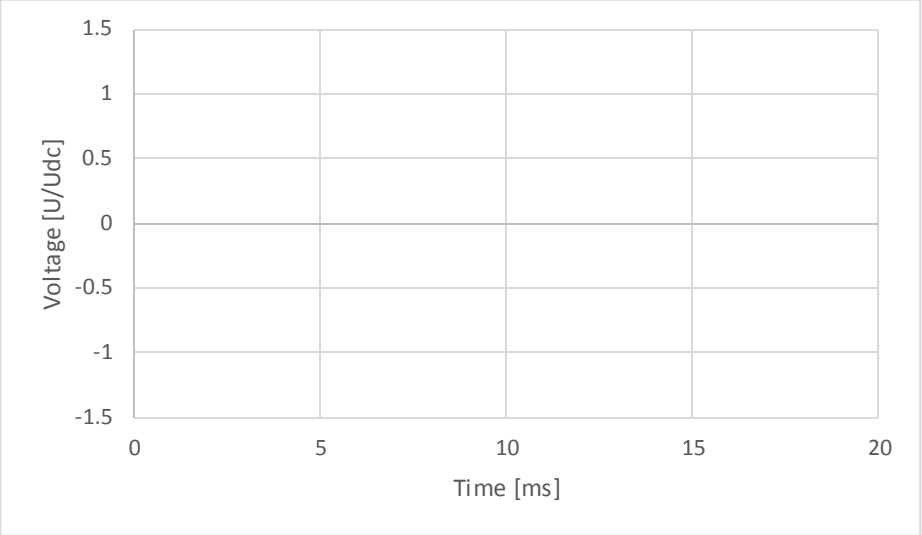

Figure 4.13 Simulated common-mode voltage at generator terminals without filtering.

Figure 4.14 shows the highest positive peaks of the simulated common-mode voltage at generator terminals with different filter inductance and capacitance values. At low values of inductance and capacitance the filter seems to have even an adverse effect on the common-mode voltage level. The voltage level starts to decrease at quite high levels of capacitance. In Figure 4.15, the voltage peaks are shown with 4 µH inductance and a wider range of capacitance. The common-mode voltage peaks decrease consistently, when the capacitance is increased, but considering the losses introduced in the results of differential-mode simulations, the advantage achieved in terms of the common-mode voltage reduction is too low. Therefore, it is reasonable to decide the filter parameters based on the differential-mode characteristics only.

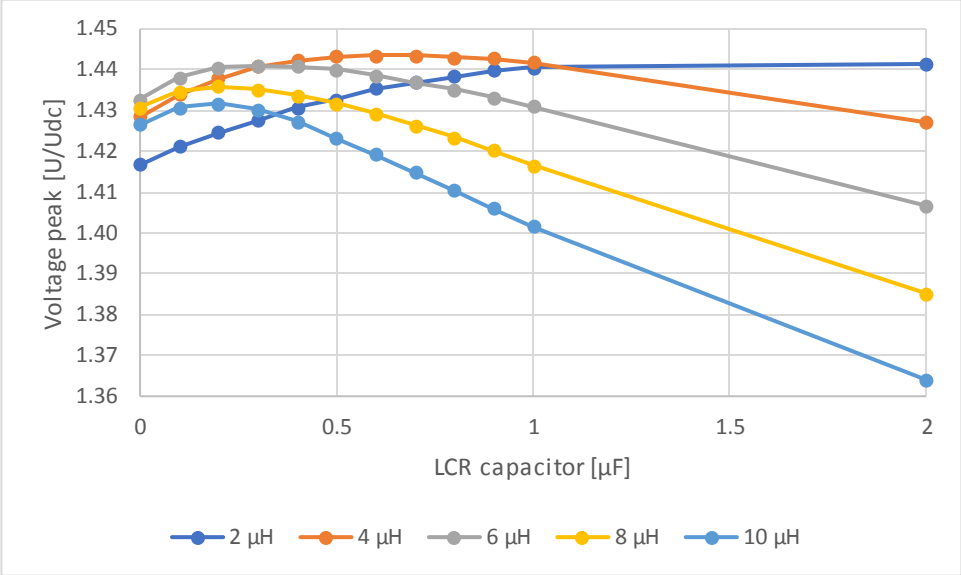

Figure 4.14 Common-mode voltage maximum peaks with different filter inductance and capacitance values.

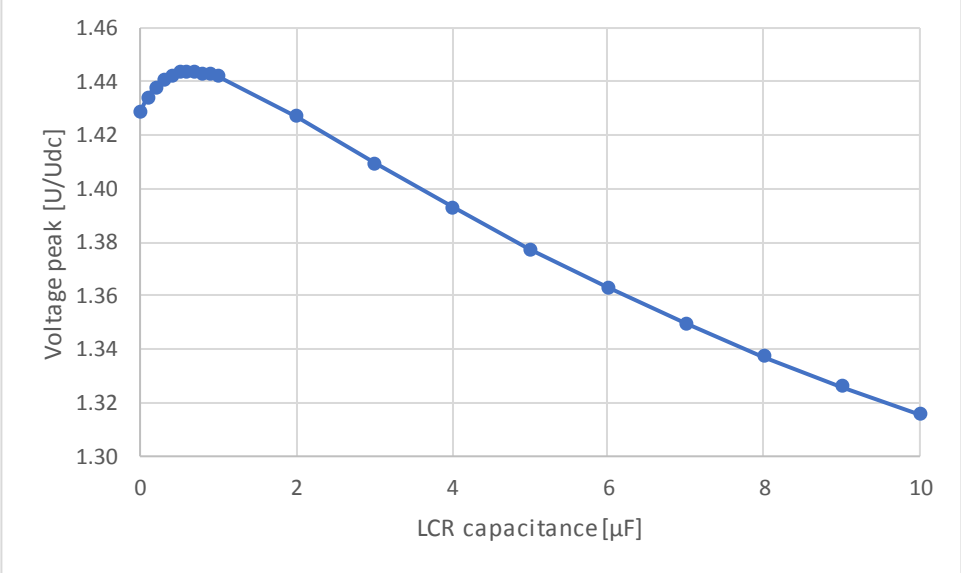

Figure 4.15 Common-mode voltage maximum peaks with 4 µH filter inductance. Larger scale of capacitance values are used than in Figure 4.14.

4.4 Simulation conclusions

Simulations confirmed that the performance of a diode clamped d*u*/d*t* filter is better than that of a conventional LCR filter both in terms of low power dissipation and filtering of differential-mode overvoltages. The LCR filter requires larger components to reach the same voltage peak suppression capability, leading to higher losses and larger physical size of the components.

As the simulations show, the common-mode impedances of any of the filters are not sufficient in filtering the common-mode voltage. A notably higher capacitance or inductance would be required, which on the other hand, would increase the losses or costs to unbearable levels. Furthermore, it should be considered that the precise value of the common-mode inductance of the inductor is not known.

The simulation model does not consider the effect of the voltage reflections to common-mode voltages. Hence the simulation results of the common-mode voltage peak magnitude primarily aim to compare different solutions and component values to each other. As discussed in section 3.2, attenuation of the generator side differential-mode voltage peaks caused by voltage reflections also affect the common-mode voltage level. Hence, a decrease in the differential-mode voltage peaks should also decrease the maximum peaks of the common-mode voltage.

The diode clamped topologies without damping resistors in d*u*/d*t* filter result in less linear graphs in simulations, when the filter parameters are altered. The clamping circuit is not as effective and fast in attenuation of oscillations as the combination of damping resistors and clamping circuit. Therefore, higher voltage spikes occur. The observations indicate that the LCR clamping circuit (Figure 3.12) is the most efficient and reliable solution investigated in this thesis. In the following considerations, the component values for the prototype filter will be decided.

Figures 4.11 and 4.12 show that a 4µH inductance seems to be inadequate to keep the maximum voltage under the defined limit of 1.45 U_{DC}. On the other hand, the benefit from increasing the phase inductance decreases significantly at about 8 µH and thus the use of much higher inductance might not be profitable. Because of the saturation of the

inductor's effect on the maximum voltage, 8 µH inductance seems to be the most adequate value considering the target of 1.45 U_{DC} voltage peak.

A higher filter capacitance value would decrease the voltage to the required level, but at the same time, increase the resistor losses significantly. According to Figure 4.12, increasing the capacitance value from 0.1 µF to 0.5 µF does not make a notable difference in terms of differential-mode overvoltage level, but the resistor losses approximately double. Therefore, the phase inductance of the filter under test will be chosen to be 8µH and 12µH. Also 4 µH will be tested in order to get more data of the effect the filter inductance.

Table 4.5 introduces numerical simulation results of the LCR diode clamp filter with the selected component values for the prototype tests. Simulated maximum voltage peaks, RC branch and clamp circuit currents of the filter are shown. As seen in Table 4.5, the inductances might be enough to achieve the target without using the filter capacitors. Applying only output inductors with the clamping circuit instead of entire LCR filter would be more simple and low-loss solution, which makes it a considerable alternative.

Table 4.5 Selected filter component values and simulation results.

LCR inductance [µH]	LCR capacitance [µF]	LCR resistance [Ω]	Voltage peak [*U*/*U*dc]	Clamp resistor current [A]	LCR resistor current [A]	Clamp resistor losses [W]	LCR resistor losses [W]	Total resistor losses [W]
4			1.55	39.00		3042		3042
4	0.1	5	1.52	41.26	5.13	3404	395	3799
4	0.1	2.5	1.52	41.94	5.89	3518	257	3775
8			1.44	37.88		2870		2870
8	0.1	5	1.39	40.25	4.62	3240	321	3560
8	0.1	2.5	1.38	40.92	5.19	3349	200	3549
12			1.37	36.79		2707		2707
12	0.1	5	1.34	39.29	4.31	3088	278	3366
12	0.1	2.5	1.34	39.87	4.76	3180	169	3349

If the desired value of voltage peaks is below 1.8 U_{DC}, LCR filter could be the simplest solution to achieve the required filtering ability. However, the same voltage level can be reached with any of the diode clamped filters and the power dissipation in the filter stays at a lower level. According to the simulations, a clamp filter requires small sized inductors

(~2µH) to the output of the converter to mitigate the voltage peaks below 1.8 U_{DC} level. All filters except the conventional LCR filter resulted in voltage peaks under 1.8 U_{DC} even with the smallest filter components.

The filter component combinations presented in Table 4.5 will be constructed from the following components.

- LCR filter inductor 4 µH
- LCR filter capacitor 0.1 µF
- LCR resistor 5 Ω

The inductance of the filter will be constructed from the required amount of 4 µH inductors in series.

According to simulations the RMS current in the RC branch of the filter is approximately 6 A, when using filter parameters 4 µH, 0.1 µF and 2.5 Ω. Hence the resistors and capacitors should be sized to withstand at least 6 A current. The selected capacitor has a maximum current RMS rating of 7 A. Therefore the capacitor should have adequate characteristics for the tests. Besides, the operating times of the drive will be few minutes with an effective air cooling.

Resistors in both clamp and LCR part of the filter will be the 5 Ω resistors introduced above. To obtain the 1 Ω resistance and a sufficient power rating, 5 resistors are placed in parallel. For the 5 Ω LCR resistance, a single resistor can be placed per phase of 2 resistors for the 2.5 Ω phase resistance.

5 PROTOTYPE MEASUREMENTS

5.1 Test setup

Prototype measurements will be performed in high power laboratory conditions, where the filter can be tested with full-scale drive equipment. The cables between the generator and the converter are of a fixed length that cannot be extended to correspond to the length of a full-scale wind turbine configuration. The distance between the generator and the converter is, nevertheless, enough to cause voltage reflections of some degree and thus relevant measurement data can be obtained for the performance analysis of the filter. The main purpose of the tests is to verify the functionality and to compare different component combinations, not to test the absolute value of resulting voltage levels. Furthermore, the differences and similarities between the measurements and simulations are important aspects to be investigated. Figure 5.1 shows the test setup used in prototype measurements. To simulate the phase-to-phase capacitances of wind turbine cabling, a long cable simulator will be connected to in parallel with cables between converter and generator.

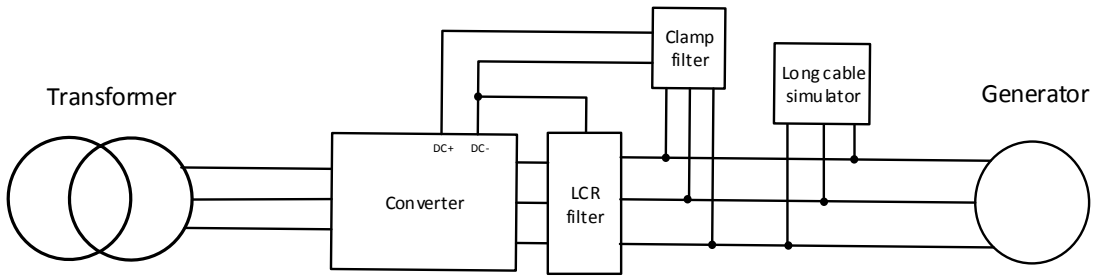

Figure 5.1 Prototype test setup

The transformer used in the test setup does not have a grounded star point. The common-mode voltage is naturally low in an ungrounded grid as explained in section 3.3. The focus of the tests will be on differential-mode voltage reduction, due to the results of the simulations. Although the magnitude of overvoltages in the laboratory conditions will not be equal to that occurring in wind turbine surroundings, the effect of the filter to the maximum voltage peaks can be investigated by comparing the results with different filter

component values and without the filter. In addition to the mentioned performance measurements of the filter, the power dissipation in filter components will be reported.

Table 5.1 lists all the different filter component values that will be tested. The prototype filter is constructed in such way that modification of the filter is simple. The RC circuit of the filter can be removed and the number of 4 µH inductors and 5 Ω resistors can be altered in order to implement the alternatives presented in Table 5.1. Measurements are first performed without any filter to obtain comparative results. In measurement number 2, the diode clamp filter is used without the LCR components. Measurements 3-11 are carried out with the entire diode clamped LCR filter.

Table 5.1 Filter setup used in the tests. Configurations 2-11 include the diode clamp filter.

Number	Filter setup
1	No filter
2	Only clamp filter
3	4 µH, No RC
4	4 µH, 0.1 µF, 5 Ω
5	4 µH, 0.1 µF, 2.5 Ω
6	8 µH, No RC
7	8 µH, 0.1 µF, 5 Ω
8	8 µH, 0.1 µF, 2.5 Ω
9	12 µH, No RC
10	12µH, 0.1 µF, 5 Ω
11	12 µH, 0.1 µF, 2.5 Ω

As noted in the previous chapter, the common-mode filtering is not effective in this type of filter with the determined component values. Therefore the measurements will focus on differential-mode overvoltages at the generator terminals and the losses in the filter components.

Both common-mode voltage and differential-mode voltages can be calculated, if the phase-to-ground voltages are measured. An oscilloscope is set to measure each phase voltage against ground at generator terminals. Also the du/dt values and the rise times of voltage pulses will be solved from the oscilloscope data.

The current through LCR filter inductors and resistors and the voltage over clamp circuit resistors will be measured for the calculations of the losses generated in the filter. The

losses in the filter capacitors are small compared to the losses in the resistors and therefore will be neglected.

5.2 Results

As expected, the differential-mode overvoltages were filtered more effectively than common-mode voltages. Figure 5.2 shows the phase-to-phase voltage waveform between U and V phases, when no filtering is applied. Differential-mode voltage spikes reach the value of approximately $2U_{DC}$ and occasionally exceed that due to the double pulsing phenomenon. The strong oscillation of the voltage is not efficiently damped by the resistance of the cabling and therefore oscillations of relatively high amplitude still occur, when the next pulse is applied by the converter. The resulting maximum value depends on the phase of the oscillation at the moment, when a switching occurs and thus coincidence has significant impact on the result.

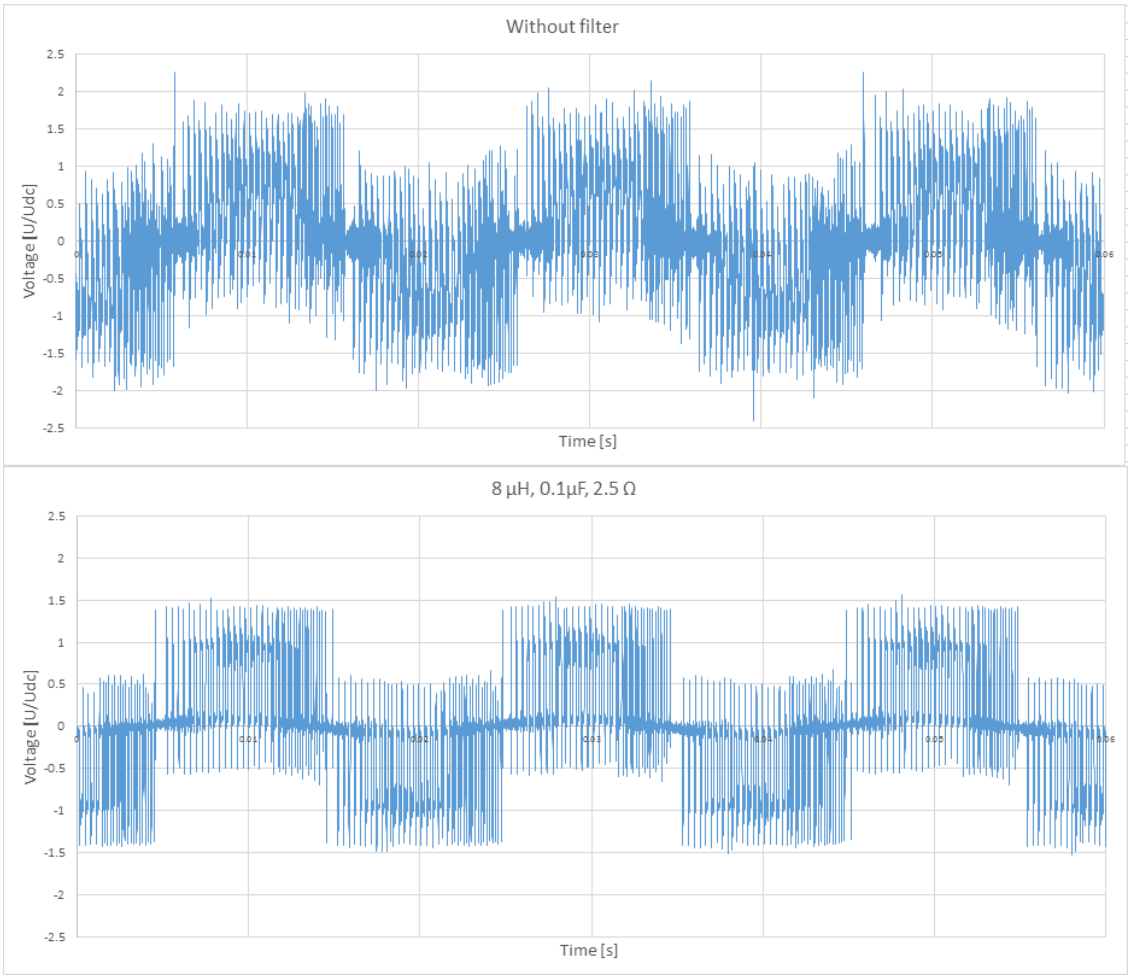

Figure 5.2 Voltage between phases U and V at the generator terminals. In the upper waveform the filter is not in use. In the lower waveform the filter components 8µH, 0.1 µF and 2.5 Ω used.

As seen in the waveforms, the highest peaks occur at a certain moment of the fundamental period during the positive and negative cycles. In Figure 5.2 the waveform of the phase-to-phase voltage shows that unusually high spikes are measured much more frequently and irregularly, when no filtering is used. Correspondingly the filtered waveform with filter setup 8 has higher spikes only at certain moments occurring twice during the fundamental period.

Figure 5.3 shows a closer zoom on the measured voltages for the purpose of investigating the behavior of the oscillating voltage waveform at the generator terminal 1) without filter, and 2) with filter setup, 3) filter setup 8 and 4) setup 9.

The strong oscillation that occurs in the unfiltered voltage waveform is quickly mitigated, when filtering is used. Compared to the simulated result in Figure 4.4 the magnitude and

the oscillation of the voltage are relatively similar. Decaying of the oscillation, however, seems to take more time in the measured one.

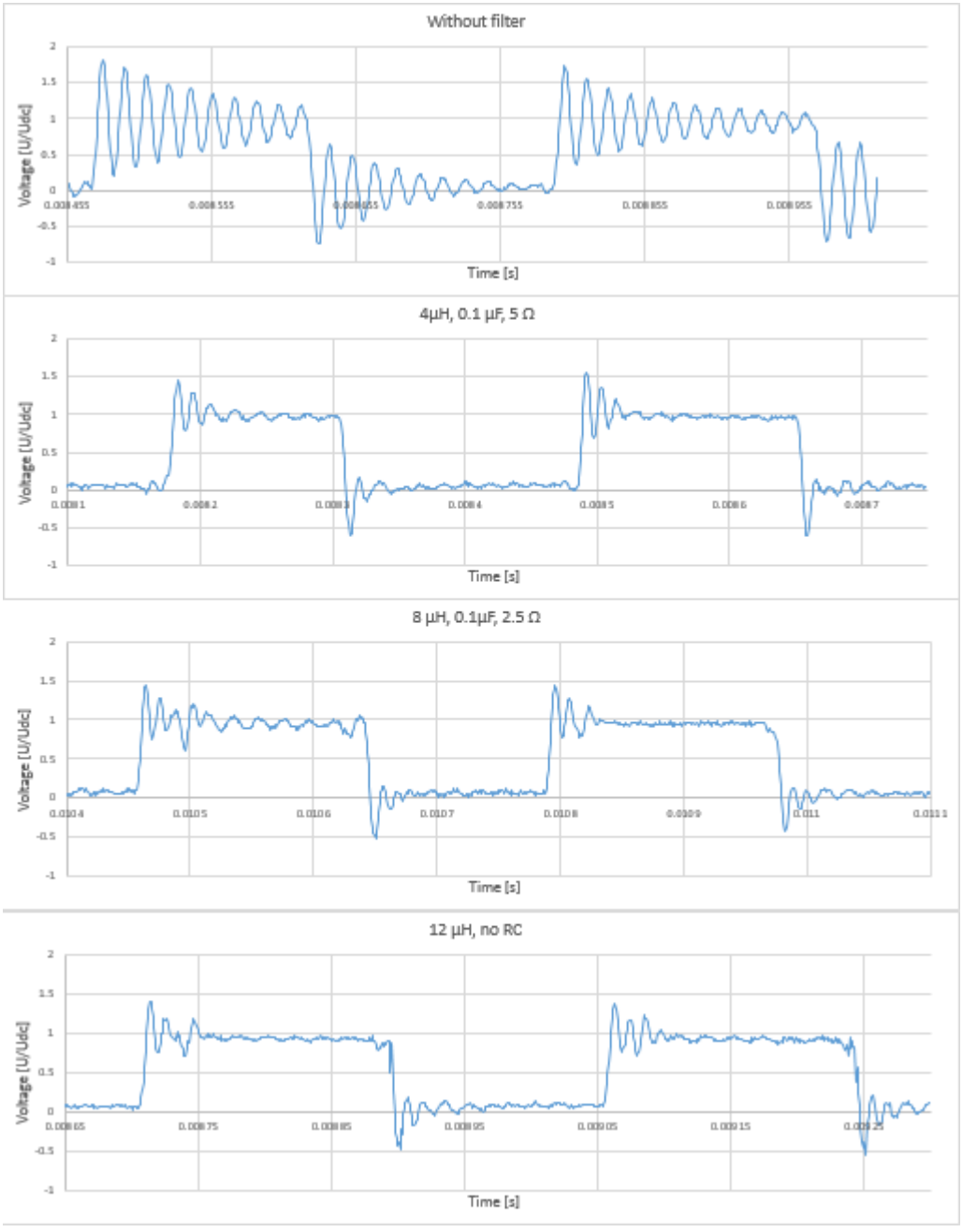

Figure 5.3 The measured voltage at generator terminals, when a pulse applied.

Figure 5.3 shows also one switching occasion without filter in which the oscillation has almost completely been suppressed before the next pulse is applied. The observation confirms the assumption that double pulsing phenomenon has a major effect on the high

voltage spikes in the unfiltered output voltage. Without the effect of double pulsing, the maximum voltage seems to rise to approximately 1.7 U_{DC}. The other graphs show a decrease of voltage spike maximum, when more filtering is added. The oscillation decays well before the next switching, although some ripple or oscillation seems to remain after the natural oscillation has been damped. That ripple, however, might be disturbance induced by voltages in proximity of the measurement devices.

Table 5.2 presents the highest positive and negative spikes measured at the generator terminals between phases U and V. The comparison between the maximum voltage spike levels of different filter component values is more relevant if the highest spikes of each fundamental period is neglected. Therefore, Table 5.2 compares the highest negative and positive value during a half period of fundamental frequency in order to avoid the highest peaks caused by double pulsing. The half period contains enough pulses to obtain the maximum and minimum peaks with different filter combinations.

The filter expectedly decreases the voltage spikes, when the inductance value is increased. On the other hand, the benefit of the RC circuit with the chosen component values seems questionable according to the measurements, since the effect to the maximum voltage peak is minor or nonexistent. Also the total power dissipation caused by the filter is shown in Table 5.2. The losses are presented more detailed in Table 5.4.

Table 5.2 Highest measured voltage peak and filter losses.

Filter setup	u_max [U/U_{DC}]	u_min [U/U_{DC}]	Total filter losses [W]
1	1.98	-2.00	-
2	1.59	-1.60	2144
3	1.53	-1.50	3183
4	1.50	-1.50	4016
5	1.50	-1.51	3869
6	1.45	-1.46	4340
7	1.44	-1.42	5010
8	1.44	-1.44	4833
9	1.41	-1.44	5409
10	1.41	-1.41	5971
11	1.41	-1.40	5788

The voltage rise time and d*u*/d*t* values are calculated using the method described at the beginning of Chapter 2. Rise time is the time in which the voltage rises from 10 % of the DC-link voltage level to 90 %. Also the calculations of d*u*/d*t* values are made according to that rise time definition.

Table 5.3 Voltage rise times and rise rates with different LCR filter component combinations

Filter	d*u*/d*t* (V/µs)	Rise time (µs)
1	545	1.6
3	266	3.3
4	241	3.7
5	269	3.3
6	235	3.7
7	216	4.1
8	230	3.8
9	217	4.1
10	190	4.6
11	205	4.3

Filter losses for each component are presented in Table 5.4. All loss calculations are based on the RMS value of the measured current or voltage and the resistance of the component.

Table 5.4 Losses in filter components.

Filter	Clamp resistor losses [W]	RC resistor losses [W]	Inductor losses [W]	Total filter losses [W]
2	2144	-	-	2144
3	2289	-	894	3183
4	2659	469	889	4016
5	2699	282	888	3869
6	2555	-	1785	4340
7	2808	425	1777	5010
8	2803	243	1787	4833
9	2706	-	2702	5409
10	2923	372	2676	5971
11	2877	224	2687	5788

Unlike in the simulations results, the clamp resistor losses increased, when a higher filter inductance was used. The inductor losses were not taken into account in the simulation chapter, in which the resistor losses in LCR and clamp parts were the object of comparison. The resistance of the inductor causes a major share of the losses, when the number of inductors is increased.

The loss calculations presented in Table 5.4 indicate that a higher value of LCR capacitance (for example 0.25 µF) could work well, since the losses in the RC branch were low and the achieved benefit insignificant. Depending on the used filter configuration, the filter losses are approximately 0.21 – 0.6 % of the nominal power of the converter.

Figures 5.5 and 5.6 illustrate the highest peak value of phase-to-phase voltages measured from the generator terminals. In addition, the filter losses are presented in the same figures. The filter setup numbering in the graphs is the same as in Table 5.1.

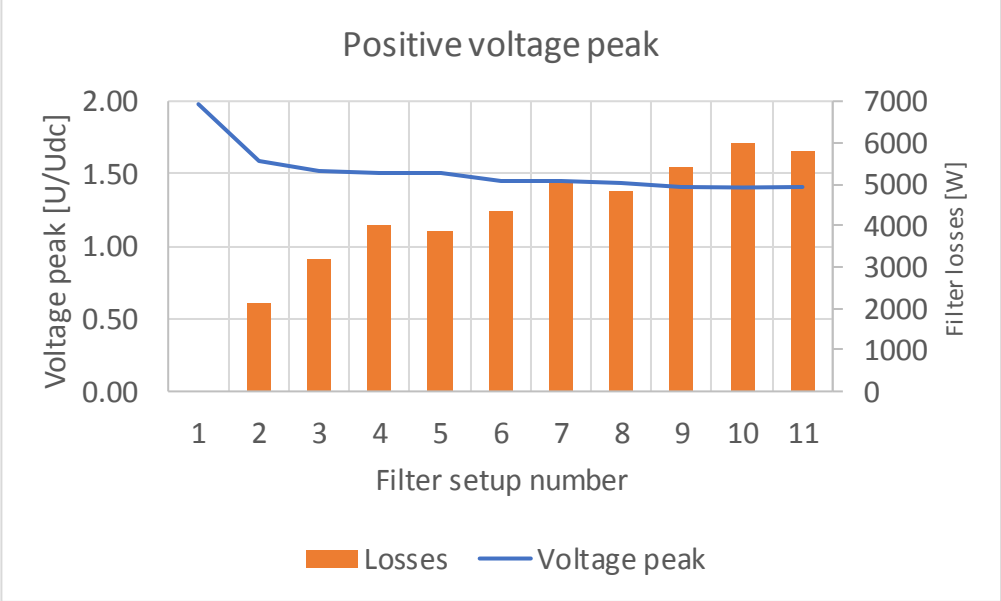

Figure 5.4 Maximum positive voltage peaks and losses with different filter component combinations.

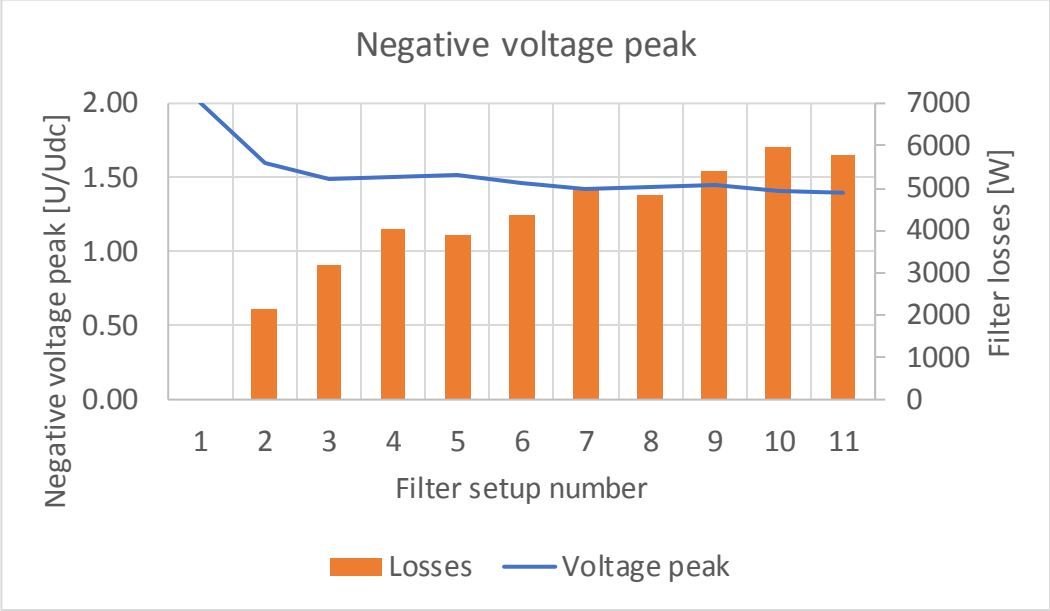

Figure 5.5 Maximum negative voltage peaks and losses with different filter component combinations.

The design in Chapter 4 aimed to decrease the maximum voltage spikes below the level of 1.82 U_{DC} and 1.45 U_{DC}. As seen in the results, without the double pulsing phenomenon occurring frequently, both goals were achieved. If the high peaks caused by double pulsing are included, even the 1.45 U_{DC} requirement is almost fulfilled, when 12 µH inductance is used. Based on these observations, it can be pointed out that by increasing the length of the shortest pulses, the highest voltages peaks could be avoided.

The magnitude of the voltage spikes is dependent on multiple factors that are listed in this thesis. Therefore it is obvious that the required filtering capability varies case by case. However, the measurements proved that the prototype filter has a significant effect on the differential-mode voltage spikes along with the rise time and du/dt of the voltage pulses.

The measurement results show that the implemented filter solution mainly functioned similarly as in simulations. As expected, increasing the inductance of the filter decreases the voltage spikes. The values of the filter components should be sized case-by-case to meet the demands. With larger LCR filter values, high filtering capability can be achieved. However, the power dissipation and component cost and size rise along with the increasing filtering performance. Hence the filter sizing is a matter of optimization between performance, costs and losses.

As mentioned, in this case the focus was on filtering of differential-mode voltages. Common-mode filtering was also in the scope of this thesis, but in the simulation part the filtering solutions were noticed to be too ineffective. To reach significant decrease in the common-mode voltage level, notably higher LCR filter capacitance would have been required. That would have caused too high losses in the filter resistors. To minimize the losses common-mode voltage filtering was neglected in the implementation of the solution.

6 CONCLUSIONS

According to the simulations an LCR filter combined with a diode clamped filter is the most effective solution presented in this thesis. To achieve equal filtering ability with a conventional LCR filter, a significantly higher inductance or capacitance value is required and thus the losses, cost, volume and weight of the filter would increase. Also sufficient common-mode filtering with the proposed filters would have increased the losses excessively. Therefore the diode clamped LCR filter was chosen for the prototype measurements, which focused on differential-mode filtering and neglected the common-mode aspect.

The filter had mostly an expected effect on the overvoltages occurring at the generator terminals. The diode clamp filter significantly decreased the level of the maximum voltage peaks. However to lower the voltage rise time and du/dt, and to further decrease the maximum voltages, du/dt filter was required. The use of filter inductance and increasing the inductance had a decreasing effect on the generator voltage peaks, whereas the amount of capacitance and resistance had no consistent effect applying to all measurement cases.

The functionality of the LCR filter combined with the diode clamp was proven with simulations and laboratory measurements. To apply the filter solution in wind turbine drives, for optimal result the dimensioning of components should be done separately for different cases taking into account the requirements and other perquisites related to the case.

REFERENCES

[1] Molina, M.G. & Alvarez J.G. 2011. Technical and Regulatory Exigencies for Grid Connection of Wind Generation. [Cited 21.12.2017] https://www.intechopen.com/books/wind-farm-technical-regulations-potential estimation-and-siting-assessment/technical-and-regulatory-exigencies-for-grid-connection-of-wind-generation

[2] Rashid, M.H. Power electronics handbook: devices, circuits, and applications. Third edition. 2011. Butterworth-Heinemann.

[3] IEA Technology Roadmap: Wind Energy. 2013. https://www.iea.org/publications/freepublications/publication/Wind_2013_Roadmap.pdf

[4] ABB Technical guide No. 7 – Dimensioning of a drive system. 2001. [Cited 21.12.2017]
https://library.e.abb.com/public/a3ef20fdc69ccc9ac12578800040ca95/ABB_Technical_guide_No_7_REVC.pdf

[5] Pyrhönen, J., Hrabovcova, V. & Semken R.S. 2016. Electrical Machine Drives Control: An Introduction. Wiley.

[6] Mohan, N., Undeland, T. M., Robbins, W. 2003. Power Electronics: Converters, Applications and Design. Wiley.

[7] Dzhankhotov, V. 2009. Hybrid LC Filter for Power Electronic Drives: Theory and Implementation. Dissertation. Acta Universitatis Lappeenrantaensis 354. Lappeenranta University of Technology, Finland.

[8] ABB Technical Guide No. 102. Effects of AC Drives on Motor Insulation. 1997. https://library.e.abb.com/public/fec1a7b62d273351c12571b60056a0fd/voltstress.pdf

[9] Saunders, L.A., Skibinski, G.L., Evon, S.T & Kempes, D.L. Riding the Reflected Wave-IGBT Drive Technology Demands New Motor and Cable Considerations. 1996 IAS Petroleum and Chemical Industry Technical Conference, pp.75-84.

[10] Kerkman, R.J., Leggate, D. & Skibinski, G.L. Interaction of drive modulation and cable parameters on AC motor transients. IEEE Transactions on Industry Applications, 1997, vol. 33, pp. 722-731.

[11] Rahman, M.F., Haider, T., Haque, E. & Blackburn T.R. 2014. A Study of the Overvoltage Stress with IGBT Inverter Waveforms on Motor and Supply Cabling and Their Remedial Measures. [Cited 21.12.2017]. https://www.researchgate.net/publication/255642944_A_STUDY_OF_THE_OVERVOLTAGE_STRESS_WITH_IGBT_INVERTER_WAVEFORMS_ON_MOTOR_AND_SUPPLY_CABLING_AND_THEIR_REMEDIAL_MEASURES

[12] Jouanne, A. & Enjeti P.N. Design Considerations for an Inverter Output Filter to Mitigate the Effects of Long Motor Leads in ASD Applications. IEEE Transactions on Industry Applications, 1997, vol. 33, pp. 1138-1145.

[13] Swamy, M.M., Yamada, K., Kume, T. Common Mode Current Attenuation Techniques for Use with PWM Drives. IEEE Transactions on Power Electronics, 2001, vol. 16, pp. 248-255.

[14] Dzhankhotov, V., Pöllänen, R., Vallinmäki, A., Alho, T. & Pyrhönen, J. 2013. Phase-to-Ground Voltage Estimation at Wind Turbine Generator Terminals. [Cited 22.2.2018] http://sgemfinalreport.fi/files/Dzhankhotov%20et%20al.pdf

[15] Lee, H.D., Sul, S.K. A common-mode voltage reduction in converter-inverter system by shifting active space vector in a sampling period. Applied Power Electronics Conference and Exposition, 1999, vol. 2, pp. 1046-1051.

[16] Skibinski, G. Design Methodology of a Cable Terminator to Reduce Reflected Voltage on AC Motors. Industry Applications Conference, 1996, vol. 1, pp. 153-161.

[17] Moreira, A., Santos, M., Lipo, T. & Venkataramanan, G. Filter Networks for Long Cable Drives and Their Influence on Motor Voltage Distribution and Common-Mode Currents. IEEE Transactions on Industrial Electronics, 2005, vol. 52, pp. 515-522.

[18] Korhonen, J. 2012. Active Inverter Output Filtering Methods. Acta Universitatis Lappeenrantaensis 482. Lappeenranta University of Technology, Finland.

[19] Dzhankhotov, V. & Pyrhönen J. Passive LC filter Design Considerations for Motor Applications. IEEE Transactions on Industrial Electronics, 2013, vol. 60, issue 10. pp. 4253-4259.

[20] Rendusara, D. & Enjeti, P. An Improved Inverter Output Filter Configuration Reduces Common and Differential Modes *dv/dt* at the Motor Terminals in PWM Drive Systems. IEEE Transactions on Power Electronics, 1998, vol. 13, issue 6, pp. 1135-1143.

[21] Rendusara, D. & Enjeti, P. A Method to Reduce Common Mode and Differential Mode dv/dt at the Motor Terminals in PWM Rectifier/PWM Inverter Type Adjustable Speed Drive Systems. Applied Power Electronics Conference and Exposition, 1998, vol. 2, pp. 1010-1016.

[22] Palma, L. & Enjeti, P. An Inverter Output Filter to Mitigate dv/dt Effects in PWM Drive System. IEEE Applied Power Electronics Conference and Exposition, 2002, vol. 1, pp. 550-556.

[23] Sayed-Ahmed, A & Sibinski G. Design and Analysis for an Integrated Differential-Common Mode Filter for On Site Motor Bearing Problems. IEEE International Electrical Machines & Drives Conference, 2011, pp. 283-288

[24] Hanigovszki, N., Poulsen, J. & Blaablerg, F. 2004. A Novel Output Filter Topology to Reduce Motor Overvoltage. IEEE Transactions on Industry Applications, 2004, vol. 40, issue 3, pp. 845-852.

[25] Habetler, T.G., Naik, R., Nondahl, T.A. Design and Implementation of an Inverter Output LC Filter Used for DV/DT Reduction. IEEE Transactions on Power Electronics, 2002, vol. 17, issue 3, pp. 327-331.

[26] Acharya, A.B. & John, V. Design of Output *dv/dt* filter for Motor Drives. 5th International Conference on Industrial and Information Systems. pp. 562-567.

[27] Hyypio, D. Mitigation of bearing electro-erosion of inverter-fed motors through passive common-mode voltage suppression. IEEE Transactions on Industry Applications, 2005, vol. 41, issue 2, pp. 576-583.

[28] Weidinger, T. & Piepenbreier, B. Analysis and Oscillations of Electrical Drive System with Active Front End and Long Motor Cables. International Symposium on Power Electronics, Electrical Drives, Automation and Motion, 2008, pp. 906-911.